Astron. Astrophys. 320, 209–227 (1997)

ASTRONOMY
AND
ASTROPHYSICS

Dynamics and gravitational wave signature of axisymmetric rotational core collapse

T. Zwerger and E. Müller⋆

Max-Planck-Institut für Astrophysik, Karl-Schwarzschild-Str. 1, Postfach 1523, D-85740 Garching, Germany

Received 8 August 1996 / Accepted 27 September 1996

Abstract. We have carried out a comprehensive parameter study of the dynamics of rotational core collapse in massive stars. The iron cores have been approximated by axisymmetric rotating $\Gamma = 4/3$ polytropes in rotational equilibrium. Any transport effects by neutrinos have been neglected. We have computed 18 initial models which differ by their amount of rotational energy and their distribution of angular momentum. The initial models range from slowly to rapidly rotating and from rigidly to extremely differentially rotating configurations. The collapse was induced by suddenly reducing the adiabatic index Γ to a value Γ_r with $1.28 \leq \Gamma_r \leq 1.325$. The stiffening of the equation of state at nuclear matter density and the thermal pressure in the matter heated by the prompt shock was simulated by means of a simplified analytic equation of state consisting of a polytropic and a thermal part. The evolution of a total of 78 models was followed well beyond core bounce using a two dimensional Newtonian hydrodynamic finite difference code.

A subset of models suffers a bounce caused by centrifugal forces at sub-nuclear densities. For a given rotation rate the bounce density decreases with increasing Γ_r and with increasing degree of differential rotation. Models suffering a bounce due to (or mainly due to) centrifugal forces show large amplitude oscillations of the inner core the central density varying by more than a factor of ten. In several models the rotation rate exceeds the critical value, where MacLaurin spheroids become secularly unstable against tri-axial perturbations. Two of the most differentially and rapidly rotating models reach ($\Gamma_r = 1.30$) and even exceed ($\Gamma_r = 1.28$) the critical value for axisymmetric dynamical stability.

We have also computed the gravitational (quadrupole) wave signal emitted by our core collapse models. We find both type I (spike + ring-down) and type II (several distinct spikes) gravitational wave signals. Which type occurs is solely determined by the adiabatic index. Signals of type I are produced by models with a "soft" equation of state ($\Gamma_r \lesssim 1.31$), while signals of type II require a "stiff" equation of state ($\Gamma_r \gtrsim 1.32$). Decreasing the adiabatic index from 1.325 to 1.28 and keeping the other model parameters fixed, we observe a smooth transformation of the signal type. For $\Gamma_r = 1.28$ a third signal type is observed, which shows a large positive and a smaller negative wave amplitude just before and after bounce. Signals of type III are not found for extremely differentially rotating initial models. The energy spectra cover a frequency range of $50\,\mathrm{Hz} \lesssim \nu \lesssim 3\,\mathrm{kHz}$, but most of the power is emitted between 500 Hz and 1 kHz. Models bouncing at sub-nuclear densities have spectra, which drop extremely rapidly above 1 kHz, and models with a type II wave signal have spectra, which show characteristic oscillations. These oscillations vanish when the signal type changes to type I. The spectra are neither very sensitive to the rotation rate nor to the degree of differential rotation. The total amount of energy radiated in form of gravitational waves lies in the range $6\ 10^{-11} M_\odot c^2 \lesssim E_{GW} \lesssim 8\ 10^{-8} M_\odot c^2$. The corresponding dimensionless wave amplitudes are in the range $4\ 10^{-25} \lesssim h \lesssim 4\ 10^{-23}$ for a source at a distance of 10 Mpc. The largest signals are either produced by models which are initially slowly rotating and have an adiabatic index $\Gamma_r \geq 1.32$, or which are initially rapidly and strongly differentially rotating and have a relatively small adiabatic index ($\Gamma_r \leq 1.30$).

Key words: gravitational waves – hydrodynamics – stars: neutron – stars: rotation – supernovae: general

1. Introduction

It is well known from observations that massive stars (spectral types O, B, A and F) have surface equatorial rotational velocities on the main-sequence in the range $100\ \mathrm{km/s} \lesssim \mathrm{v\,sin(i)} \lesssim 300$ km/s, where i is the inclination angle between the axis of rotation and the light of sight (for a review, see e.g., Tassoul (1978). However, the initial angular momentum distribution and its evolution with time are unknown. The latter is determined by the amount of angular momentum transport occurring during the stars' lifetime. If transport of angular momentum is inefficient, the increasing compactification of the central regions of the evolving massive star would lead to relatively rapidly rotating iron cores, even if the star was rotating slowly on the main-

Send offprint requests to: E. Müller

⋆ e-mail: emueller@MPA-Garching.MPG.de

sequence (Endal & Sofia 1977). If, on the other side, magnetic fields or shear viscosity are able to reduce the angular momentum in the interior of the star sufficiently, its iron core will rotate slowly. Unfortunately, evolutionary calculations of rotating massive stars up to the stage of core collapse, which could help to narrow down the range of initial (i.e., pre-collapse) angular momenta of iron cores, have not yet been performed.

In spite of the unknown rotational state of the iron core prior to collapse, several attempts have been made in the past two decades to study the influence of rotation on the dynamics of core collapse by means of hydrodynamic simulations (LeBlanc & Wilson 1970; Müller et. al. 1980; Tohline et. al. 1980; Müller & Hillebrandt 1981; Symbalisty 1984; Finn & Evans 1990; Mönchmeyer et. al. 1991; Marck & Bonazzola 1992; Bonazzola & Marck 1993; Mönchmeyer 1993; Yamada & Sato 1994, 1995; Zwerger 1995; Müller & Zwerger 1995). All of these simulations, except those recently performed by Zwerger (1995), were restricted to a few specific core collapse models incorporating a more or less sophisticated treatment of the complicated micro physics and transport processes involved in the event.

We have followed up a somewhat complementary approach. We have restricted ourselves to a simplified description of the micro physics and have approximated the iron cores by rotating polytropes neglecting any transport effects. Thereby we have been able to perform a truly comprehensive parameter study of the space spanned by possible pre-collapse iron core models. A related, but much less comprehensive approach has been pursued by Yamada & Sato (1994, 1995). Contrary to all previous investigations, except those of Bonazzola & Marck (1993, 1994), we have also used rotating equilibrium configurations as initial models. We have further analyzed the gravitational radiation emitted by the collapsing rotating cores and computed the emitted gravitational (quadrupole) wave signal including amplitudes, spectra and radiated energies.

The paper is organized as follows. In the next section we discuss some general aspects of rotational core collapse. In Sect. 3 we describe our numerical model in detail and in Sect. 4 we present the results of our parameter study concerning the dynamics of rotational core collapse. The gravitational wave signal emitted during rotational core collapse models is discussed in Sect. 5. Finally, in Sect. 6 we summarize our results, discuss shortcomings arising from the approximations made in our numerical model and point out implications and necessary improvements for future investigations.

2. General considerations

Core collapse without rotation has been extremely well studied during the past two decades (for a review, see e.g., Bethe 1990; Müller 1990; Bruenn 1993). It is now generally accepted that the collapse proceeds approximately adiabatically and will only be stopped when the central density reaches nuclear matter density. The stiffness of the nuclear equation of state causes a bounce of the core and the formation of a shock wave. This prompt shock is created at the edge of the inner core. The latter is defined as that inner part of the iron core which collapses subsonically. While propagating outward through the supersonically infalling outer core the prompt shock is severely weakened due to energy losses by photo-disintegration of heavy nuclei into free nucleons and by neutrino losses. Hence, within several milliseconds after core bounce the prompt shock stalls and turns into an accretion shock. According to the delayed explosion mechanism (Wilson 1985) after some hundred milliseconds the stalled prompt shock is revived. This occurs due to energy deposition in the post shock layers by neutrinos diffusing out of the nascent neutron star. The re-energized shock then causes a supernova explosion.

We point out here that in our study the shock revival phase has not (and also could not) been considered, mainly because we did not include any neutrino transport effects in our numerical model (see next section). The main aim of our investigation was not to provide realistic supernova models, but to study the influence of rotation on the dynamics of core collapse and to predict the range of expected waveforms, signal strengths and spectra of gravitational radiation from rotational core collapse.

The most important difference between the collapse of rotating and non-rotating cores is that in rotating cores centrifugal forces may stop the collapse *before* nuclear matter density is reached. This possibility was pointed out by Shapiro & Lightman (1976) and discussed in more detail by Tohline (1984) and Eriguchi & Müller (1984). Numerical examples of such a low-density bounce have been given by several authors (Müller et. al. 1980; Symbalisty 1984; Mönchmeyer 1993; Yamada & Sato 1994; Zwerger 1995).

A theoretical argument for the stabilizing influence of rotation on (pseudo-) radial modes of stars was derived by Ledoux (1945). To guarantee the stability of a configuration in rotational equilibrium the adiabatic index

$$\gamma \equiv \frac{\partial \ln P}{\partial \ln \varrho}|_{Y_e,s} \tag{1}$$

defined as the logarithmic derivative of the pressure P with respect to the density ϱ at fixed entropy s and electron fraction Y_e should fulfill the condition

$$\gamma > \gamma_{crit} = \frac{2}{3}\,\frac{(2-5\beta)}{(1-2\beta)} \tag{2}$$

the rotation parameter β being defined by

$$\beta = \frac{E_{rot}}{|E_{pot}|}\ . \tag{3}$$

Here E_{rot} and E_{pot} are the rotational and potential energy, respectively. Although Eq. (2) was derived for slow rigid rotators with Γ independent of density, numerical calculations have shown that Eq. (2) holds under more general conditions, too (see e.g., Tassoul 1978). Moreover, Eq. (2) is only applicable if corrections due to general relativity are small (i.e., if $GM/Rc^2 \ll 1$). Otherwise, the general relativistic analogue of Eq. (2) must be used (see e.g., Tassoul 1978, chap. 14). Compared to the Newtonian one the relativistic criterion gives a larger γ_{crit}, because general relativity tends to destabilize configurations.

For a given (average) γ the critical value of β a rotating core in equilibrium must exceed to be stable against pseudo-radial modes is

$$\beta > \beta_{crit} = \frac{1}{2}\,\frac{(4-3\gamma)}{(5-3\gamma)}\,. \tag{4}$$

This is also a necessary condition for a core bounce to occur at sub-nuclear densities (Tohline 1984; Mönchmeyer 1993). We point out here that the stability and hydrodynamic evolution of a collapsing core is actually determined by the *effective* adiabatic index

$$\Gamma \equiv \left.\frac{\partial \ln P}{\partial \ln \varrho}\right|_M, \tag{5}$$

which describes the change of pressure along a collapse trajectory of a given mass element (van Riper & Lattimer 1982). Hence, γ must be substituted by Γ in Eqs. (2) and (4).

Due to conservation of angular momentum the centrifugal forces increase significantly during collapse. Matter in the equatorial plane does not fall towards the center as fast as matter at the polar axis leading to a progressive flattening of the core. In addition, the collapse time scale is lengthened compared to non-rotating models.

Conservation of angular momentum may also lead to very rapidly rotating configurations, which are unstable against tri–axial deformations on secular or even dynamical time scales. For MacLaurin spheroids, i.e., for incompressible, rigidly rotating equilibrium configurations, secular and dynamical tri–axial instabilities grow, if $\beta \geq 13.75\,\%$ and $\beta \geq 27.38\,\%$, respectively (see e.g., Tassoul 1978). Whether these instabilities do indeed occur (and if so, at which values of β) in compressible, differentially rotating stars is still an open question. If the equation of state at sub–nuclear densities is stiff, i.e., if the adiabatic index is very close to 4/3, the core may be stabilized before its rotational energy exceeds the critical value. If, on the other side, the initial amount of rotation is small enough for the collapse to proceed to nuclear densities, the critical value of β may not be reached before bounce.

After bounce a rotating core oscillates with a superposition of various radial and surface modes (Mönchmeyer 1993). The frequency of these modes is determined by the average density of the inner core. In contrast to a spherically symmetric core, which comes to rest soon after bounce, in a rotating core a certain fraction of its kinetic infall energy will be converted into oscillations, which are damped by non-spherical pressure waves. These oscillations strongly contribute to the gravitational wave signal of the bouncing core.

3. Numerical model

3.1. Equation of state

We approximate the collapsing core by a rotating polytrope in order to examine a large set of initial conditions and use a simplified analytic equation of state (Janka et. al. 1993) neglecting all transport effects. The equation of state consists of a *polytropic* part P_p and a *thermal* part P_{th}

$$P = P_p + P_{th}. \tag{6}$$

The polytropic part P_p accounts for pressure contributions due to degenerate, relativistic electrons and (at high densities) due to the repulsive action of nuclear forces. P_{th} mimics the thermal pressure in the matter heated up by the prompt shock. Writing P as a sum of these two terms prevents matter elements from following the same P-ϱ-history during infall and expansion after bounce. Two different density regimes are considered, where

$$P_p = \begin{cases} K_1\,\varrho^{\Gamma_1}, & \text{if} \quad \varrho \leq \varrho_{\rm nuc} \\ K_2\,\varrho^{\Gamma_2}, & \text{otherwise.} \end{cases} \tag{7}$$

The *nuclear density* $\varrho_{nuc} = 2\;10^{14}\,\mathrm{g/cm^3}$, the *supra-nuclear* adiabatic index $\Gamma_2 = 2.5$, and the value of K_1 is fixed to

$$K_1 = \frac{3}{4}\,(\frac{\pi}{3})^{2/3}\,\hbar c\,(\frac{Y_e}{m_B})^{4/3} = \;1.2435\,10^{15}\,Y_e^{4/3}\,\mathrm{cgs}, \tag{8}$$

which holds for an ideal gas of ultra-relativistic, degenerate electrons (i.e., $\Gamma_1 = 4/3$; see e.g., Shapiro & Teukolsky 1983). In Eq. (8), Y_e is the mean number of electrons per baryon (or electron number fraction) and the other quantities have their usual meaning. From the first law of thermodynamics the corresponding thermodynamically consistent energy density follows (for adiabatic changes) as

$$u_p = \begin{cases} E_1\,\varrho^{\Gamma_1}, & \text{if} \quad \varrho \leq \varrho_{nuc} \\ E_2\,\varrho^{\Gamma_2} + E_3\,\varrho, & \text{otherwise.} \end{cases} \tag{9}$$

where E_1 and E_2 are related to K_1 and K_2 by

$$K_1 \;=\; (\Gamma_1 - 1)\,E_1, \tag{10}$$

$$K_2 \;=\; (\Gamma_2 - 1)\,E_2. \tag{11}$$

The constants E_2 (and hence K_2) and E_3 are fixed by requiring continuity of P_p and u_p at ϱ_{nuc}. This leads to

$$E_2 \;=\; \frac{\Gamma_1 - 1}{\Gamma_2 - 1}\,E_1\,\varrho_{nuc}^{\Gamma_1-\Gamma_2}, \tag{12}$$

$$E_3 \;=\; \frac{\Gamma_2 - \Gamma_1}{\Gamma_2 - 1}\,E_1\,\varrho_{nuc}^{\Gamma_1-1}. \tag{13}$$

The thermal pressure P_{th} is related to the thermal energy density u_{th} by an ideal gas relation

$$P_{th} = (\Gamma_{th} - 1)\,u_{th}, \tag{14}$$

with $\Gamma_{th} = 1.5$ corresponding to a mixture of relativistic and non-relativistic gases. The total energy density

$$u = u_p + u_{th}. \tag{15}$$

Initially u_{th} and P_{th} are zero and should remain so in the absence of shocks. Further details are given in Janka et. al. (1993).

Before bounce the typical electron number fraction $Y_e \gtrsim 0.32$ and the specific entropy $s \lesssim 1.5\,\mathrm{k}_B$/nucleon (Bruenn

1993). For these conditions realistic equations of state (see e.g., , Hillebrandt & Wolff 1985, Lattimer & Swesty 1991) have an adiabatic index $1.30 \lesssim \Gamma \lesssim 1.33$ for densities 10^{10} g/cm^3 $< \varrho <$ $1.5\,10^{14}$ g/cm^3. For supra-nuclear densities ($\varrho > 2\,10^{14}$ g/cm^3) and modest entropies ($1\ k_B/\text{nucleon} \lesssim s \lesssim 2\ k_B/\text{nucleon}$) the equation of state stiffens considerably, the adiabatic index rising to $2.5 \lesssim \Gamma \lesssim 3.0$.

3.2. Initial models

Contrary to all previous studies, except those of Bonazzola & Marck (1993,1994), the initial models are in rotational equilibrium being calculated with the method of Eriguchi & Müller (1984). All initial models are $\Gamma = 4/3$ axially symmetric polytropes with a central density of $\varrho_c = 10^{10}$ g/cm^3 and an electron number fraction $Y_e = 0.5$.

Initially all models rotate according to the rotation law (Eriguchi & Müller 1984)

$$\Omega(\widetilde{\omega}) = \Omega_0 \left[1 + (\frac{\widetilde{\omega}}{A})^2\right]^{-1}, \qquad (16)$$

where $\widetilde{\omega}$ is the distance from the rotation axis. The constant Ω_0 is uniquely related to the rotational energy of the initial model specified by the rotation parameter β_i (see Eq. (3), while A is an additional independent free parameter determining the initial angular momentum distribution. For large values of A (compared to the size of the initial model) one obtains almost rigidly rotating configurations, while small values of A correspond to strongly differentially rotating ones. We computed a set of 18 initial models, which were obtained by combining four different initial angular momentum distributions (A1 – A4) and five different initial rotation parameters (B1 – B5; see Table 1). For $A = 5\ 10^9$ cm and $\beta_i \gtrsim 1\,\%$ no equilibrium models exist, because in these rapidly rotating rigid rotators the rotational velocity exceeds the Keplerian velocity in the outer layers. The strongly differentially ($A = 10^7$ cm) and rapidly ($\beta_i \geq 1.8\,\%$) rotating initial models (see Table 1) have an off-center density maximum, i.e., they have a torus-like density stratification with $\varrho_{max}/\varrho_{cen} = 1.05$ (model A4B4) and 1.30 (model A4B5),respectively.

The collapse of the rotating equilibrium models was induced by suddenly reducing Γ to a value Γ_r. We studied the collapse for five different values of Γ_r (G1 – G5): 1.325, 1.32, 1.31, 1.30, and 1.28, respectively.

In the parameter space spanned by A, β_i and Γ_r, we have computed a total of 78 models (see Tables 2 and 3) and followed their evolution well beyond core bounce. For convenience, we will refer to a specific model according to the following scheme: A1B2G3 denotes the model with the parameters A = A1 = $5\ 10^9$ cm, β_i = B2 = 0.49 % and Γ_r = G3 = 1.31, respectively.

3.3. Hydrodynamics

The hydrodynamic evolution of the models was calculated in spherical coordinates using a modified version of the multidimensional Newtonian hydrodynamic code PROMETHEUS developed by Fryxell & Müller (Fryxell et. al. 1989) and based on the Piecewise Parabolic Method (PPM) of Colella & Woodward (1984). PROMETHEUS has successfully passed various standard one and two-dimensional tests. In addition, Janka et. al. (1993) have compared PROMETHEUS with a 1D Lagrangian code including a tensor artificial viscosity. They have studied the spherical core collapse of polytropes and obtained nearly identical results. As PROMETHEUS is further designed to exactly (i.e., up to machine accuracy) guarantee the global conservation properties of the hydrodynamic equations, it also conserves total angular momentum, which is important for rotational core collapse.

We assumed both axial and equatorial symmetry. The computational domain was covered by a non-equidistant moving grid in radial direction with $N_r = 360$ zones. The moving grid was necessary in order to adequately resolve both the center of the polytrope and the edge of the unshocked inner core, where the shock wave forms during core bounce. Thus, the radial grid was contracted (and after bounce expanded) with the inner core, such that there were always 180 radial zones within the radius of the inner core R_{ic} containing a mass M_{ic}. In angular direction we used an equidistant Eulerian grid with $N_\Theta = 18$ zones, i.e., an angular resolution of 5 degrees.

Newtonian self-gravity was taken into account by expanding the formal integral solution of Poisson's equation into Legendre polynomials up to order 10 and utilizing a computationally effi-

Table 1. Properties of the computed initial models, which are all axisymmetric rotating $\Gamma = 4/3$ polytropes in rotational equilibrium with a central density of 10^{10} gcm^{-3}. The model parameters A and β_i specify the angular momentum distribution (see Eq. (16) and the relative amount of rotational energy (see Eq. (3). R_{eq}, M and J give the equatorial radius, the mass and the angular momentum of the configuration. The equatorial radius and mass of a corresponding non-rotating 4/3 polytrope are $1.554\,10^8$ cm and $1.457\ M_\odot$, respectively.

Initial model	A [10^8 cm]	β_i [%]	R_{eq} [10^8 cm]	M [$M_\odot$]	J [10^{49} erg s]
A1B1	50	0.26	1.634	1.463	1.24
A1B2	50	0.49	1.727	1.473	1.73
A1B3	50	0.90	2.224	1.491	2.42
A2B1	1.0	0.25	1.580	1.463	1.19
A2B2	1.0	0.45	1.600	1.471	1.61
A2B3	1.0	0.89	1.645	1.491	2.35
A2B4	1.0	1.79	1.745	1.533	3.54
A2B5	1.0	4.00	2.026	1.648	6.23
A3B1	0.5	0.24	1.563	1.462	1.09
A3B2	0.5	0.48	1.571	1.473	1.58
A3B3	0.5	0.89	1.583	1.491	2.19
A3B4	0.5	1.80	1.609	1.534	3.29
A3B5	0.5	4.00	1.663	1.649	5.64
A4B1	0.1	0.25	1.536	1.463	0.77
A4B2	0.1	0.48	1.518	1.473	1.09
A4B3	0.1	0.90	1.487	1.492	1.52
A4B4	0.1	1.80	1.419	1.535	2.26
A4B5	0.1	4.00	1.255	1.658	3.85

cient recursion relation for the resulting radial integrals (Müller & Steinmetz 1995).

To check for grid resolution effects, we performed five simulations with an increased number of computational zones. In two simulations (rigidly rotating models A1B1G1 and A1B3G2) we doubled the number of radial zones (N_r = 720) and in two other simulations (differentially rotating models A3B1G2 and A3B4G3) we used a finer angular grid with N_Θ = 45 corresponding to an angular resolution of 2 degrees. In the fifth simulation we recalculated the evolution of the extremely differentially and rapidly rotating model A4B5G5 with an angular grid of N_Θ = 90 zones. These simulations showed that our standard grid resolution (N_r = 360 and N_Θ = 18) gives sufficiently accurate results except for the case of extremely rapidly ($\beta_i \gtrsim 2\,\%$) and extremely differentially (A = A4 = 10^7 cm) rotating models.

Increasing the radial grid resolution mainly improves the conservation of the total energy, which cannot exactly be conserved numerically. This is due to the non-conservative nature of the gravity terms in the hydrodynamic equations (see e.g., Müller & Steinmetz 1995). For model A1B1G1 the error in the total energy is reduced from 50 % to 22 % and for model A1B3G2 from 28 % to 13 % when doubling the number of radial zones. Although being seemingly large, the errors in the conservation of the total energy are not critical at all, because the total energy is small compared to the individual energies (e.g., $\lesssim 0.5\%$ of the absolute value of the gravitational binding energy). Thermal energy, gravitational binding energy and mass quadrupole moment differ by less than 1 %, the bounce density by about 1 %, the kinetic energy ($\lesssim 20\%$ of the thermal energy) by a few percent and the energy radiated in form of gravitational waves by up to 15 %.

An increased angular resolution does only slightly improve the total energy conservation. The differences found for the individual energies and the quadrupole moment are somewhat larger when increasing the angular resolution than when increasing the radial one. An adequate angular resolution is most important for rapidly and differentially rotating models. However, even in the most extreme model A4B5G5, the gravitational wave amplitude and the amount of energy radiated in form of gravitational waves differ by less than 15% when increasing the angular resolution from N_Θ = 18 to N_Θ = 90. The bounce and post-bounce central density is very inaccurately determined (up to a factor of 10 off) at low angular resolution in rapidly and extremely differentially rotating models (A = A4 = 10^7 cm), because of their torus-like density stratification. Our comparison runs show, however, that this inaccuracy is not important for the dynamics of the core, because it affects only the (relatively) low density region inside the torus-like off-center density maximum, i.e., the "surface layers" of the torus.

3.4. Gravitational wave signal

The gravitational wave signal has been calculated using a post-Newtonian approach, where numerically troublesome higher order time derivatives of the quadrupole moment are transformed into much better tractable spatial derivatives. In particular, the gravitational quadrupole radiation field, $h^{\rm TT}$, is calculated with an expression derived independently by Nakamura & Oohara (1989), and by Blanchet et. al. (1990):

$$h_{ij}^{\rm TT}(\boldsymbol{X},t) \;=\; \frac{2G}{c^4 R} P_{ijkl}(\boldsymbol{N}) \;\times \int d^3x\;\varrho\left[2v^k v^l - x^k\;\partial_l\Phi - x^l\;\partial_k\Phi\right], \qquad (17)$$

where $R = |\boldsymbol{X}|$ is the distance between the observer and the source, Φ is the Newtonian gravitational potential, ϱ is the mass-density and $\boldsymbol{v}$ is the velocity. The other quantities have their usual meanings except for $P_{ijkl}(\boldsymbol{N})$ (with $\boldsymbol{N} = \boldsymbol{X}/R$) which denotes the transverse-traceless (TT) projection operator onto the plane orthogonal to the outgoing wave direction $\boldsymbol{N}$, acting on symmetric Cartesian tensors according to

$$P_{ijkl}(\boldsymbol{N}) \;=\; (\delta_{ik} - N_i N_k)\,(\delta_{jl} - N_j N_l) \;-\; \frac{1}{2}(\delta_{ij} - N_i N_j)\,(\delta_{kl} - N_k N_l)\,. \qquad (18)$$

∂_i represents the partial derivative with respect to the x^i coordinate. The integrand in Eq. (17) is defined on a compact manifold and is known to the (2nd order) accuracy level of the numerical algorithm of the hydro-code.

It can be easily shown that evaluating the integral of Eq. (17) by an integration scheme (of at least 2nd order) is by one order of accuracy superior to twice applying numerical time-differentiation methods to quadrupole data given at discrete points of time (Finn & Evans 1990, Mönchmeyer et. al. 1991).

For 2D (axisymmetric) simulations, which are most conveniently performed in spherical coordinates, it is natural to represent the (total) radiation field $\widetilde{h}^{\rm TT}$ in terms of the "pure-spin tensor harmonics" $T_{ij}^{{\rm E2},lm}$ and $T_{ij}^{{\rm B2},lm}$ with amplitudes $A_{lm}^{\rm E2}$ and $A_{lm}^{\rm B2}$ in the following way (Thorne 1980):

$$\widetilde{h}_{ij}^{\rm TT}(\boldsymbol{X},t) = \frac{1}{R}\sum_{l=2}^{\infty}\sum_{m=-l}^{+l}\Big\{\; A_{lm}^{\rm E2}\;(t-\frac{R}{c})\,T_{ij}^{{\rm E2},lm}(\theta,\phi) + \;+\; A_{lm}^{\rm B2}\;(t-\frac{R}{c})\,T_{ij}^{{\rm B2},lm}(\theta,\phi)\Big\} \qquad (19)$$

In spherical coordinates the coefficients $A_{lm}^{\rm E2}$ and $A_{lm}^{\rm B2}$ have especially simple integral representations over the source. By symmetry, there is only one non-vanishing quadrupole term in Eq. (19), namely $A_{20}^{\rm E2}$. Higher-order terms are neglected in the quadrupole approximation $h^{\rm TT}$ of the gravitational radiation field $\widetilde{h}^{\rm TT}$. Transforming Eq. (17) to spherical coordinates and expressing v_i in terms of unit vectors in the r, θ and ϕ direction, one obtains by comparison of Eq. (17) with the lowest-order term of Eq. (19) for the (mass) quadrupole wave amplitude $A_{20}^{\rm E2}$ the expression

$$A_{20}^{\rm E2}(t) \;=\; \frac{G}{c^4}\frac{16\pi^{3/2}}{\sqrt{15}}\int_{-1}^{1}\int_{0}^{\infty}\varrho(r,z,t)\Big[v_r v_r(3z^2-1) \;+ \;+\, v_\theta v_\theta(2-3z^2) - v_\phi v_\phi - 6 v_r v_\theta z\sqrt{1-z^2} \;+$$

$$- r\partial_r\Phi\,(3z^2-1) + 3\partial_\theta\Phi\, z\sqrt{1-z^2}\Big] r^2 dr dz\ , \quad (20)$$

where $\partial_r = \partial/\partial r$, $\partial_\theta = \partial/\partial\theta$, and $z = \cos\theta$.

From the definition of $T_{ij}^{\mathrm{E2},2m}$ (Thorne 1980, Eq. (2.39e)) one derives for the components of h^{TT} the formula

$$h_{\theta\theta}^{\mathrm{TT}} = \frac{1}{8}\sqrt{\frac{15}{\pi}}\,\sin^2\theta\,\frac{A_{20}^{\mathrm{E2}}(t)}{R} \;\equiv\; h_+\ . \quad (21)$$

The only other nonzero component is $h_{\phi\phi}^{\mathrm{TT}} = -h_{\theta\theta}^{\mathrm{TT}}$. Note that due to the hypotheses of (i) axisymmetry and (ii) of Newtonian gravity $h_{\theta\theta}^{\mathrm{TT}} = h_+$ and $h_\times = 0$, where h_+ and $h_\times$ are the wave amplitudes corresponding to the two independent polarizations of the gravitational radiation field (see, e.g., Shapiro & Teukolsky 1983, chap. 16).

The total energy radiated in gravitational waves is then given by

$$E_{GW} = \frac{c^3}{G}\frac{1}{32\pi}\int_{-\infty}^{+\infty}\left(\frac{dA_{20}^{\mathrm{E2}}}{dt}\right)^2 dt\ . \quad (22)$$

The energy radiated per unit frequency $dE/d\nu$ can be calculated from the amplitude A_{20}^{E2} using the fast Fourier transform technique.

4. Results: dynamics of rotational core collapse

4.1. Initial models in rotational equilibrium

All previous calculations of rotational core collapse, except those of Bonazzola & Marck (1993, 1994), used spherically symmetric initial models to which a certain amount of rotational energy was added without allowing for a relaxation of the model before collapse. Hence, these initial models are not in a state of rotational equilibrium. It was argued that, as long as the added amount of rotation is sufficiently small, this should cause no large errors for the dynamics of rotational core collapse (see, e.g., Müller 1982). In order to check the validity of this commonly made statement quantitatively, we have compared the collapse of a polytrope in rotational equilibrium with that of the corresponding rotating, spherically symmetrical, non-equilibrium polytrope.

For the comparison we selected three models: A2B1G1, A2B3G2 and A2B4G3. These models have the same initial angular momentum distribution, but have different initial rotation rates ($\beta_i = 0.25\,\%, 0.89\,\%$ and $1.79\,\%$) and different reduced adiabatic indices ($\Gamma_r = 1.325, 1.32$ and 1.31). In case of the non-equilibrium initial models we choose the rotation law parameter Ω_0 (see Eq. (16)) in such a way that the initial (relative) rotational energy β_i but *not* the initial angular momentum J agreed with that of the corresponding equilibrium polytrope.

For the same central density a rotating polytrope has a larger equilibrium mass than a non-rotating one (see Table 1). Hence, if a non-equilibrium polytrope is allowed to relax before collapse, it will evolve towards an equilibrium configuration at a lower central density. This behaviour is reflected in our simulations, where we observe a slight expansion of the models for $1-2$ ms before the initial pressure reduction (due to lowering the adiabatic index from Γ to Γ_r) causes the model to collapse eventually. The dynamical behaviour of models in rotational equilibrium is different, because they collapse immediately.

During collapse the non-equilibrium models try to approach an angular density stratification in accordance with the centrifugal forces. Whether this stratification can be achieved depends on the time until core bounce (when the adjustment process ends), which is mainly determined by the reduced adiabatic index Γ_r. The closer Γ_r is to the limiting value 4/3 (i.e., the smaller the initial pressure reduction is), the slower the collapse proceeds. In addition, the smaller the initial rotation rate β_i, the smaller is the initial deviation from rotational equilibrium, and hence the shorter is the time required for the adjustment of the angular density stratification.

For the initially slowly rotating model A2B1G1 ($\beta_i = 0.25\,\%$), which bounces at $t_b = 93.4$ ms, the deformation (as measured by the quadrupole moment of the configuration) of the equilibrium and the non-equilibrium model agree very well for $t \gtrsim 75$ ms. For the initially more rapidly rotating model A2B3G2 ($\beta_i = 0.89\,\%$), which also experiences a larger initial pressure reduction ($\Gamma_r = 1.32$ instead of $\Gamma_r = 1.325$ in model A2B1G1), the earlier bounce ($t_b = 71.3$ ms) prevents the non-equilibrium model from adjusting its angular density stratification before bounce completely. However, the post-bounce evolution of the equilibrium and non-equilibrium model is very similar. In case of model A2B4G3 ($\beta_i = 1.79\,\%$, $\Gamma_r = 1.31$) the adjustment of the stratification cannot be achieved before bounce ($t_b = 50.3$ ms). In this most unfavourable case (of the three investigated models) the evolution of the non-equilibrium model deviates significantly from that of the equilibrium model. Nevertheless, if one is only interested in rough estimates of characteristic model quantities (e.g., the bounce density or the rotational energy at bounce), the non-equilibrium model still provides acceptable results.

The central densities at bounce differ in models A2B1G1 and A2B3G2 by about 1 % and in model A2B4G3 by about 10 %. The differences in the potential and thermal energies are below 1 % for the first two models and reach a few percent for the third model. The kinetic energies (which are small compared to the potential or thermal energy) of the equilibrium models are larger than those of the non-equilibrium ones by up to 15 % and the rotational energies are smaller by several percent. The larger kinetic energy of the equilibrium models at bounce gives rise to more energetic shock waves, because the initial shock energy is approximately equal to the kinetic energy of the inner core at bounce (see, e.g., Mönchmeyer 1993). For all three models the masses and the angular momenta of the inner cores of the equilibrium and non-equilibrium models differ by less than 0.1 %. For models A2B1G1 and A2B3G2 the radius of the inner cores of the non-equilibrium models is almost the same as that of the equilibrium models, while it is smaller by about 10 % in case of model A2B4G3.

The comparison shows that the usage of non-equilibrium initial models is justified, if the core can establish an angular density stratification before bounce, which is in accordance with

Table 2. Overview of collapse simulations of initially rigidly (A = A1 = 5 10^9 cm) or almost rigidly (A = A2 = 10^8 cm) rotating configurations (see Eq. (16 and Table 1). Γ_r is the adiabatic index to which the initial models' adiabatic index ($\Gamma = 4/3$) is reduced to initiate core collapse. t_b, ϱ_b and β_b are the time, central density and rotation parameter at bounce. M_{ic}, J_{ic} and T_{ic} are the mass, angular momentum and equatorial rotation period of the inner core at bounce. t_f, ϱ_f and β_f are the time, central density and rotation parameter, when either the simulation was stopped or when mass began to flow off the grid due to the outward propagating shock wave (denoted by an asterix in the last column). A_{20}^{E2} and E_{GW} are the (absolute) maximum value of the gravitational quadrupole wave amplitude and the total amount of energy radiated in form of gravitational waves.

Model	Γ_r	t_b [ms]	ϱ_b [10^{14} gcm^{-3}]	β_b [%]	M_{ic} [$M_\odot$]	J_{ic} [10^{49} erg s]	T_{ic} [ms]	t_f [ms]	ϱ_f [10^{14} gcm^{-3}]	β_f [%]	A_{20}^{E2} [10^3cm]	E_{GW} [10^{-8} $M_\odot c^2$]	
A1B1G1	1.325	93.1	3.26	5.4	1.09	0.49	2.4	101.4	2.41	3.6	-1.89	6.5	
A1B1G2	1.320	69.2	3.49	4.2	0.86	0.29	2.4	74.7	2.62	3.0	-1.02	2.2	
A1B1G3	1.310	48.3	3.81	2.9	0.50	0.10	2.6	51.6	2.90	2.2	-0.33	0.21	
A1B1G4	1.300	38.7	4.03	2.1	0.29	0.04	2.7	44.7	3.07	1.6	-0.11	0.039	
A1B1G5	1.280	29.8	4.47	1.2	0.11	0.01	2.7	42.7	3.35	1.0	+0.04	0.006	
A1B2G1	1.325	94.2	2.87	8.3	1.19	0.84	3.0	105.6	2.55	7.1	-2.24	4.7	
A1B2G2	1.320	69.7	3.23	7.1	0.90	0.44	2.2	74.8	2.25	4.5	-1.77	5.1	
A1B2G3	1.310	48.5	3.64	5.1	0.54	0.15	2.4	59.2	2.66	3.7	-0.60	0.85	
A1B2G4	1.300	38.8	3.94	3.7	0.31	0.05	2.2	43.3	2.99	2.8	-0.20	0.13	
A1B2G5	1.280	29.9	4.32	2.1	0.11	0.01	2.6	42.3	3.26	1.8	+0.07	0.013	
A1B3G1	1.325	96.1	1.73	10.1	1.22	1.20	5.6	126.4	0.15	4.5	-1.32	0.88	*
A1B3G2	1.320	70.5	2.79	10.6	0.99	0.71	2.8	107.9	1.38	6.7	-2.12	5.3	*
A1B3G3	1.310	48.8	3.36	8.1	0.57	0.23	2.0	59.5	2.46	5.7	-1.05	2.8	
A1B3G4	1.300	39.0	3.72	6.2	0.35	0.09	1.9	54.6	2.58	4.5	-0.34	0.43	
A1B3G5	1.280	30.0	4.23	3.5	0.11	0.01	1.8	41.6	3.19	3.1	+0.13	0.043	
A2B1G1	1.325	93.4	3.08	6.4	1.16	0.64	2.7	106.2	2.56	5.0	-2.23	6.0	
A2B1G2	1.320	69.4	3.36	5.5	0.89	0.37	2.4	76.9	2.48	3.8	-1.34	3.9	
A2B1G3	1.310	48.4	3.75	4.2	0.52	0.13	2.4	51.7	2.85	3.1	-0.49	0.51	
A2B1G4	1.300	38.8	3.97	3.2	0.31	0.05	2.3	44.6	3.02	2.4	-0.18	0.10	
A2B1G5	1.280	29.9	4.38	1.8	0.10	0.01	2.7	42.2	3.29	1.5	+0.06	0.012	
A2B2G1	1.325	94.6	2.56	9.4	1.21	0.96	3.7	122.4	0.10	2.8	-2.12	4.5	*
A2B2G2	1.320	70.0	3.05	8.7	0.95	0.56	2.5	75.7	2.35	6.5	-2.16	5.8	
A2B2G3	1.310	48.6	3.49	6.9	0.56	0.20	2.1	58.2	2.58	4.9	-0.89	2.1	
A2B2G4	1.300	38.9	3.84	5.4	0.32	0.07	1.9	43.7	2.89	3.9	-0.33	0.35	
A2B2G5	1.280	30.0	4.25	3.0	0.11	0.01	2.1	41.9	3.21	2.5	+0.10	0.035	
A2B3G1	1.325	97.0	0.70	10.6	1.25	1.45	9.6	128.7	0.44	8.9	-1.12	0.37	*
A2B3G2	1.320	71.3	2.19	12.6	1.03	0.94	4.3	90.6	0.19	5.3	-1.57	1.4	
A2B3G3	1.310	49.2	3.00	11.6	0.65	0.36	2.1	60.7	2.14	8.0	-1.45	3.3	
A2B3G4	1.300	39.3	3.40	9.3	0.37	0.13	2.5	55.6	2.29	6.7	-0.67	1.3	
A2B3G5	1.280	30.1	4.00	5.5	0.12	0.02	1.6	41.8	2.92	4.7	+0.18	0.10	
A2B4G2	1.320	73.3	0.36	13.6	1.09	1.50	10.1	115.0	0.08	7.9	-0.98	0.25	*
A2B4G3	1.310	50.3	1.87	15.8	0.71	0.62	4.0	79.7	0.42	9.4	-1.12	0.84	
A2B4G4	1.300	39.9	2.78	15.1	0.46	0.26	2.1	50.1	1.27	9.9	-0.81	1.0	
A2B4G5	1.280	30.4	3.54	9.4	0.15	0.03	1.5	41.3	2.60	8.7	+0.30	0.22	
A2B5G4	1.300	41.2	0.78	18.2	0.51	0.48	4.8	77.7	0.22	13.6	-0.49	0.22	
A2B5G5	1.280	31.1	2.66	15.3	0.17	0.07	1.7	40.3	1.11	14.3	+0.52	0.21	

its rate of rotation. This is the case for models, which initially rotate slowly ($\beta_i \lesssim 1$ %) and which, for a given rate of rotation, collapse slowly enough, i.e., where Γ_r is sufficiently close to 4/3.

4.2. Time of bounce

The time of bounce t_b is defined as the moment when the central density reaches a (first) maximum. It mainly depends on the initial pressure reduction, i.e., on the value of the reduced adiabatic index Γ_r. Using a least square fit the time of bounce of our models is well prescribed by the relation

$$t_b(\Gamma_r) = (4/3 - \Gamma_r)^{-1} t_1 + t_0 \,, \tag{23}$$

where t_1 = 20.99 ms and t_0 = 0.63 ms and where the most rapidly rotating models with β_i = 0.4 % have not been taken into account, because they show the largest deviations from the above fit. If the models with β_i = 0.4 % are included, the value of t_0 has to be increased by 0.13 ms. Models with Γ_r = 1.28 have systematically shorter times of bounce. In addition, t_b

Table 3. Same as Table 2 but for all simulations with initially differentially (A = A1 = 5 10^7 cm) or extremely differentially (A = A2 = 10^7 cm) rotating configurations. Note that for model A4B5G5 the data are taken from the simulation with N_Θ = 90 and that for this model the value of ϱ_f = 3.6 10^{10} gcm^{-3}.

Model	Γ_r	t_b [ms]	ϱ_b [10^{14} gcm^{-3}]	β_b [%]	M_{ic} [$M_\odot$]	J_{ic} [10^{49} erg s]	T_{ic} [ms]	t_f [ms]	ϱ_f [10^{14} gcm^{-3}]	β_f [%]	A_{20}^{E2} [10^3cm]	E_{GW} [10^{-8} $M_\odot c^2$]	
A3B1G1	1.325	93.5	3.01	7.1	1.19	0.72	3.6	105.2	0.48	3.1	-2.39	8.2	
A3B1G2	1.320	69.4	3.25	6.8	0.90	0.44	2.6	74.8	2.28	4.8	-1.78	5.4	
A3B1G3	1.310	48.5	3.60	6.0	0.56	0.18	2.2	51.6	2.78	4.5	-0.79	1.6	
A3B1G4	1.300	38.9	3.84	5.1	0.32	0.07	2.1	41.7	2.94	3.7	-0.35	0.34	*
A3B1G5	1.280	30.0	4.22	3.1	0.11	0.01	2.1	42.6	3.10	2.3	+0.09	0.044	
A3B2G1	1.325	95.2	2.06	10.3	1.23	1.10	6.4	124.8	0.09	3.7	-1.56	1.7	*
A3B2G2	1.320	70.4	2.62	11.5	1.02	0.77	3.7	87.6	1.15	7.3	-2.23	5.1	
A3B2G3	1.310	49.1	3.06	10.6	0.64	0.34	2.2	66.7	1.97	7.3	-1.55	3.8	
A3B2G4	1.300	39.2	3.49	9.2	0.37	0.13	1.8	43.4	2.60	6.8	-0.76	1.8	
A3B2G5	1.280	30.1	3.90	5.8	0.12	0.02	1.6	42.6	2.82	4.4	+0.17	0.13	
A3B3G1	1.325	97.5	0.39	10.9	1.27	1.58	14.2	128.5	0.06	5.7	-1.03	0.28	*
A3B3G2	1.320	72.2	0.97	13.2	1.07	1.14	7.2	102.2	0.25	8.3	-1.38	0.83	
A3B3G3	1.310	49.9	2.29	15.4	0.72	0.56	3.2	72.5	0.62	8.7	-1.40	1.7	
A3B3G4	1.300	39.7	2.81	14.5	0.46	0.26	2.0	50.6	1.42	9.4	-0.97	1.6	
A3B3G5	1.280	30.4	3.46	9.5	0.16	0.04	1.6	41.9	2.48	7.5	+0.25	0.27	
A3B4G2	1.320	74.9	0.15	14.4	1.13	1.83	15.8	107.0	0.05	9.7	-0.90	0.15	*
A3B4G3	1.310	51.9	0.46	17.0	0.78	0.94	8.3	89.7	0.14	11.2	-0.89	0.34	*
A3B4G4	1.300	41.5	1.03	17.7	0.51	0.44	4.3	87.2	0.29	11.4	-0.69	0.37	*
A3B4G5	1.280	31.0	2.58	15.1	0.21	0.09	1.7	43.7	1.10	11.8	+0.39	0.25	
A3B5G4	1.300	44.9	0.14	20.8	0.58	0.88	11.5	77.4	0.04	15.5	-0.53	0.13	*
A3B5G5	1.280	32.4	0.39	19.5	0.25	0.21	5.2	81.5	0.13	14.6	+0.70	0.13	*
A4B1G1	1.325	92.6	2.54	7.3	1.21	0.62	7.9	109.6	0.13	2.8	-1.74	3.9	
A4B1G2	1.320	69.1	2.66	8.4	1.01	0.50	5.7	79.1	1.18	6.1	-1.94	4.7	
A4B1G3	1.310	48.6	2.60	10.4	0.69	0.32	4.0	69.0	1.38	7.9	-1.66	5.0	
A4B1G4	1.300	39.2	2.53	12.1	0.47	0.20	4.5	69.5	1.22	8.3	-1.24	3.1	
A4B1G5	1.280	30.5	2.43	13.3	0.22	0.08	1.8	47.3	1.02	6.9	-0.69	1.2	
A4B2G1	1.325	92.9	1.20	9.9	1.25	0.90	13.1	119.2	0.18	5.6	-1.14	0.65	*
A4B2G2	1.320	69.5	1.69	12.1	1.05	0.74	10.9	96.3	0.16	5.7	-1.83	2.7	*
A4B2G3	1.310	48.9	1.95	15.1	0.72	0.48	7.6	81.6	0.35	8.9	-2.07	4.3	*
A4B2G4	1.300	39.6	1.92	17.3	0.51	0.32	5.1	74.4	0.44	10.2	-1.74	3.6	
A4B2G5	1.280	31.0	2.29	18.9	0.24	0.13	1.7	47.0	0.20	8.4	-1.11	2.2	
A4B3G1	1.325	92.7	0.24	10.5	1.29	1.28	25.5	119.5	0.02	4.6	-0.79	0.14	*
A4B3G2	1.320	69.4	0.44	13.3	1.10	1.07	12.8	94.6	0.04	6.2	-1.26	0.58	*
A4B3G3	1.310	49.2	0.63	17.2	0.78	0.72	7.6	76.7	0.14	10.8	-1.52	1.3	*
A4B3G4	1.300	39.9	0.70	19.8	0.58	0.50	3.6	70.4	0.13	11.4	-1.46	1.6	*
A4B3G5	1.280	31.6	0.66	22.6	0.31	0.24	1.9	82.1	0.09	9.7	-1.33	2.0	*
A4B4G2	1.320	68.2	0.09	14.7	1.18	1.67	20.9	89.8	0.02	9.2	-0.98	0.17	*
A4B4G3	1.310	48.5	0.16	19.1	0.88	1.20	8.8	68.9	0.02	10.8	-1.52	0.77	*
A4B4G4	1.300	39.7	0.21	22.5	0.62	0.80	5.4	60.5	0.02	12.9	-1.79	1.5	*
A4B4G5	1.280	31.9	0.22	27.8	0.45	0.54	2.3	52.6	0.03	12.1	-2.14	2.8	*
A4B5G4	1.300	37.4	0.06	27.9	0.80	1.70	7.9	49.0	0.01	16.9	-3.11	2.6	*
A4B5G5	1.280	30.7	0.03	34.9	0.37	0.69	3.6	40.1	0.00	19.5	-3.88	7.8	*

slightly increases with increasing rotation rate, because centrifugal forces decelerate the collapse.

4.3. Bounce

A collapsing rotating core bounces either when (i) the maximum density (which is not necessarily equal to the central density!) of the core exceeds nuclear matter density and the equation of state stiffens (see Sect. 3.1), or when (ii) centrifugal forces, which increase during collapse because of angular momentum conservation, bring the collapse to a halt (see Sect. 2). Which type of bounce occurs and at which maximum density it takes place depends on all three model parameters A, β_i and Γ_r. Note that a bounce may also occur due to a combination of both effects.

In most models the maximum density at bounce ϱ_b^{max} is reached in the center of the core. However, in the most rapidly rotating models with $A = 5\,10^7$ cm (i.e., models A3B5G4 and A3B5G5) and in all extremely differentially rotating models ($A = 10^7$ cm) the maximum density at bounce is achieved off-center. While the maximum density at bounce is only $\approx 3\,\%$ larger than the central density in models A3B5, it exceeds the central density by up to 50 % in models A4B1. For even more rapidly rotating models the density ratio increases up to a factor of 3, 5 and 7.5 for the models A4B2, A4B3 and A4B4, respectively. In the most extreme models the maximum density at bounce is 20 times (A4B5G4) or even 60 times (A4B5G5) larger than the central density.

The value of the central density at bounce ϱ_b varies from $4.5\,10^{14}\,\mathrm{gcm}^{-3}$ down to $3\,10^{12}\,\mathrm{gcm}^{-3}$ with $\varrho_b > 10^{13}\,\mathrm{gcm}^{-3}$ in all but three models (see Tables 2 and 3). In these latter models the maximum density at bounce ϱ_b^{max} exceeds $10^{13}\,\mathrm{gcm}^{-3}$. A subset of models suffers a bounce due to centrifugal forces at sub-nuclear densities. For given β_i the bounce density decreases with increasing Γ_r and decreasing A, and for given Γ_r it decreases with increasing β_i (see Tables 2 and 3). Hence, rapidly and differentially rotating models with Γ_r sufficiently close to 4/3 have low maximum (and even lower central) densities at bounce; e.g., $\varrho_b^{max} = 1.5$, 1.4 and $1.9 \times 10^{13}\,\mathrm{gcm}^{-3}$ for models A3B4G2, A3B5G4 and A4B4G2, respectively. But even for quite rigidly rotating configurations with $A = 10^8$ cm the collapse is stopped in some cases well below nuclear matter density, e.g., $\varrho_b = 3.6\,10^{13}\,\mathrm{gcm}^{-3}$ for $\beta_i = 0.018$ and $\Gamma_r = 1.32$ (A2B4G2), and $\rho_b = 7.0\,10^{13}\,\mathrm{gcm}^{-3}$ for $\beta_i = 0.9\%$ and $\Gamma_r = 1.325$ (A2B3G1).

4.4. The inner core

During core collapse of non-rotating polytropes a coherently, subsonically and homologously collapsing central region forms, which is called the inner core (Goldreich & Weber 1980; Yahil 1983). During rotational core collapse an inner core forms, too, provided the initial rotation rate is not to large (Mönchmeyer 1993). However, in the rotational case the time-dependent constant appearing in the relation between the radial infall velocity v_r and the radial coordinate r of a mass element depends on the angular coordinate, i.e., $v_r = \alpha(t, \Theta)\, r$. The value of α monotonically decreases with increasing polar angle Θ, because centrifugal forces slow down the collapse most effectively near the equator. Initially the angular variation of α is small, but it increases up to a factor of two shortly before bounce. The homology relation holds for rotational core collapse until bounce near the equator, but becomes invalid near the rotation axis for central densities exceeding $10^{12}\,\mathrm{gcm}^{-3}$. Our simulations show that these (qualitative) findings are independent of A, β_i and Γ_r.

The mass of the inner core at bounce, M_{ic}, most sensitively depends on the value of the reduced adiabatic index Γ_r. It also depends, but less strongly, on the initial rate of rotation and on the initial angular momentum distribution (see Tables 2 and 3). The dependence of M_{ic} on Γ_r is well known from spherical core collapse simulations (Yahil 1983). A lower value of Γ_r implies a larger initial pressure reduction and, hence, a faster collapse. Consequently, the size of the region of the core, which can stay in contact by sound waves, will decrease, i.e., the inner core will become smaller. A faster infall will also increase the ram pressure against which the inner core expands after bounce. Thus, in models with small values of Γ_r the inner core will hardly oscillate. This behaviour is confirmed by our simulations.

According to Tables 2 and 3, M_{ic} also slightly increases with β_i and the degree of differential rotation (i.e., with decreasing A). The first result is due to the fact that for the same central density rotation can stabilize more massive configurations. Using the virial theorem, one can show that rotation acts in some way like a gas with an adiabatic index of 5/3 (see, e.g., Shapiro & Teukolsky 1983).

The mass of a white dwarf in rotational equilibrium can roughly be estimated with the help of the virial theorem (see, e.g., Shapiro & Teukolsky 1983):

$$M = M_0\,(1 - 2\beta)^{-3/2}, \tag{24}$$

where M_0 is the mass of the corresponding non-rotating white dwarf. Setting $M = M_{ic}(t_b)$ and $\beta = \beta(t_f)$ (instead of $\beta_{ic}(t_f)$ which is not accessible), we find a rather good agreement between the inner core masses of our initially almost rigidly rotating models ($A \geq 10^8$ cm) and those predicted by Eq. (24).

The angular momenta of the inner cores (see Tables 2 and 3) obey quite accurately the exponential law

$$J_{ic} = J_0(A)\, \exp\left[\sigma(A)\, \Gamma_r\right], \tag{25}$$

where $J_0(A)$ and $\sigma(A)$ are quantities depending only on the initial angular momentum distribution. The ratio J_{ic} to the total angular momentum J is a monotonically increasing function of Γ_r and the degree of differential rotation. For the rigidly rotating models (A = A1) the ratio J_{ic}/J increases from 0.5 % to 35 %, when Γ_r is increased from 1.28 to 1.325. For A = A2 the ratio increases from 0.9 % to 60 %, for A = A3 from 2 % to 70 %, and for A = A4 from 15 % to 80 %, respectively. This behaviour is caused by the enhanced central concentration of the angular momentum in the differentially rotating models, and also by their larger inner cores.

The equatorial rotation period of the inner cores at bounce is also given in Tables 2 and 3. For small values of the reduced adiabatic index ($\Gamma_r = 1.28$) the rotation periods are in the range $1.5\,\mathrm{ms} \lesssim T_{ic} \lesssim 3.0\,\mathrm{ms}$. The rotation periods become larger with increasing Γ_r, the effect being strongest for initially rapidly rotating models. This can be explained by the larger radii of the rapidly rotating inner cores.

4.5. Evolution of the central density

In most models bouncing above nuclear matter density the inner core exhibits only a few, small amplitude (variation of the central density $\lesssim 20\%$) post-bounce radial oscillations around the final rotational equilibrium configuration, which is established within several milliseconds after core bounce. Only the inner cores of models with $\Gamma_r \geq 1.32$ experience a large number of

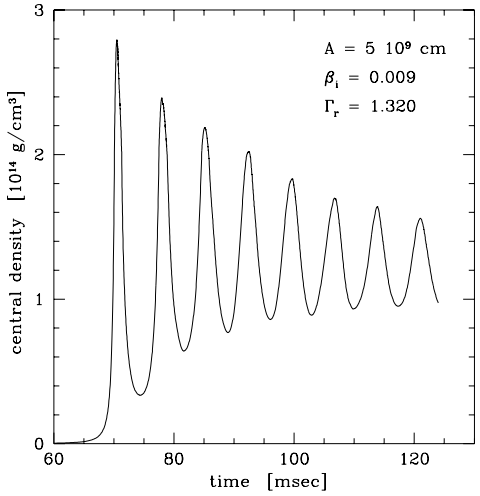

Fig. 1. Central density as a function of time for model A1B3G2. This model bounces above nuclear matter density and shows very regular, damped radial oscillations with a period of 7.2 ms.

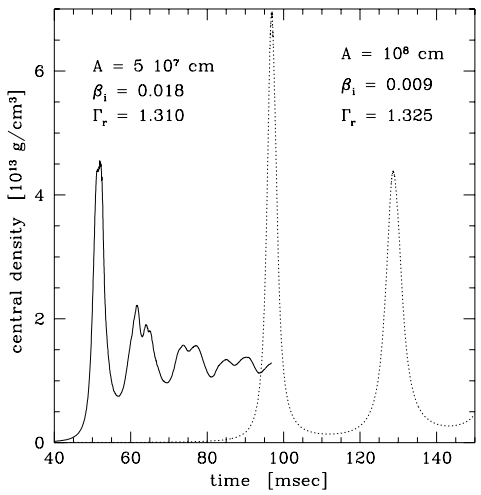

Fig. 2. Central density as a function of time for models A3B4G3 (solid curve) and A2B3G1 (dotted curve). Both models bounce due to centrifugal forces at sub-nuclear matter densities and exhibit large amplitude post-bounce radial oscillations of the inner core.

weakly damped radial oscillations of considerable initial amplitude (with a factor of 5 to 10 variation in the central density). The central density of such a model (A1B3G2) is shown in Fig. 1 as a function of time. The oscillation period is nearly constant. It has a value of about 7.2 ms except for the first oscillation, which has a slightly longer period. The central density drops from $2.8\,10^{14}\,\mathrm{gcm}^{-3}$ at bounce to $3.4\,10^{13}\,\mathrm{gcm}^{-3}$ during the first re-expansion and then again increases to $2.4\,10^{14}\,\mathrm{gcm}^{-3}$ at the second bounce (see Fig. 1), i.e., the central density at the second bounce is a factor 0.83 smaller than at the first bounce. During subsequent bounces the central density decreases by an almost constant factor of 0.94, which implies a damping time scale of ≈ 120 ms.

Models bouncing due to (or mainly due to) centrifugal forces show large amplitude radial oscillations of the inner core. The central density varies by more than a factor of ten in such models. For example, in model A3B4G3 (solid curve in Fig. 2) the bounce density is $\varrho_b = 4.6\,10^{13}\,\mathrm{gcm}^{-3}$. Then the model re-expands, the central density dropping down to $\varrho = 7.5\,10^{12}\,\mathrm{gcm}^{-3}$. Eventually the model achieves a new equilibrium state with a central density of $\varrho = 1.3\,10^{13}\,\mathrm{gcm}^{-3}$. Even more extreme is model A2B3G1 (dotted curve in Fig. 2), where the central density drops by about a factor of 50 from $6.9\,10^{13}\,\mathrm{gcm}^{-3}$ (at bounce) to $1.4\,10^{12}\,\mathrm{gcm}^{-3}$ (at maximum re-expansion) and then rises again by about a factor of 30 to $4.4\,10^{13}\,\mathrm{gcm}^{-3}$ during the second bounce (see Fig. 2).

The central density at the end of the simulations, ϱ_f, when the inner core is nearly in rotational equilibrium, is given in Tables 2 and 3. Its dependence on the three model parameters A, β_i and Γ_r is quite similar to that of the bounce density ϱ_b. Note in this respect that in all models marked with an asterix in the last column of Tables 2 and 3, ϱ_f is the central density at the moment when mass begins to flow off the grid due to the outward propagating shock wave. Hence, in these models the final rotational equilibrium state could not be computed. For models bouncing above nuclear matter density we find $\varrho_f \approx 0.4\varrho_b$, while models experiencing a centrifugal bounce have $\varrho_f \approx 0.1\varrho_b$ due to the "softer" restoring force of rotation (see Sect. 4.4).

4.6. Evolution of the rotation rate

Because of angular momentum conservation the effects of rotation become more important during collapse, which is reflected by an increase of the value of β. Fig. 3 shows the rotation rates β_b of all models at core bounce as a function of the initial rotation rate β_i., the four panels corresponding to the four different initial angular momentum distributions.

For several models β exceeds the critical value $\beta_{\mathrm{sec}} = 13.75\,\%$, where MacLaurin spheroids become secularly unstable against tri-axial perturbations (see Tables 2 and 3). In three models (A3B5G4, A4B3G5 and A4B4G4) β becomes larger than 20 %, but stays below the critical value for dynamical instability ($\beta_{\mathrm{dyn}} = 27.38\,\%$). In none of the initially rigidly rotating models ($A = 5\,10^9$ cm) the rotation rate exceeds the critical value for secular instability. Most of the secularly unstable models with $A \leq 10^8$cm, $\beta_i \geq 0.9\,\%$ and $\Gamma_r \leq 1.32$ remain in the unstable regime for several milliseconds, and for $\beta_i = 4.0\,\%$ even for several tens of milliseconds (see Fig. 4). Whether this time is long enough to allow for a significant growth of the secular instability is, however, unclear.

Three of the most differentially rotating ($A = 10^7$ cm), most rapidly collapsing ($\Gamma_r \leq 1.30$) and most rapidly rotating initial models ($\beta_i \geq 1.8\%$) reach (models A4B4G5 and A4B5G4) and even considerably exceed (model A4B5G5) the critical value for dynamical stability β_{dyn} (see Figs. 3 and 4, and Tables 2 and 3). However, in the latter case β remains larger than β_{dyn} only

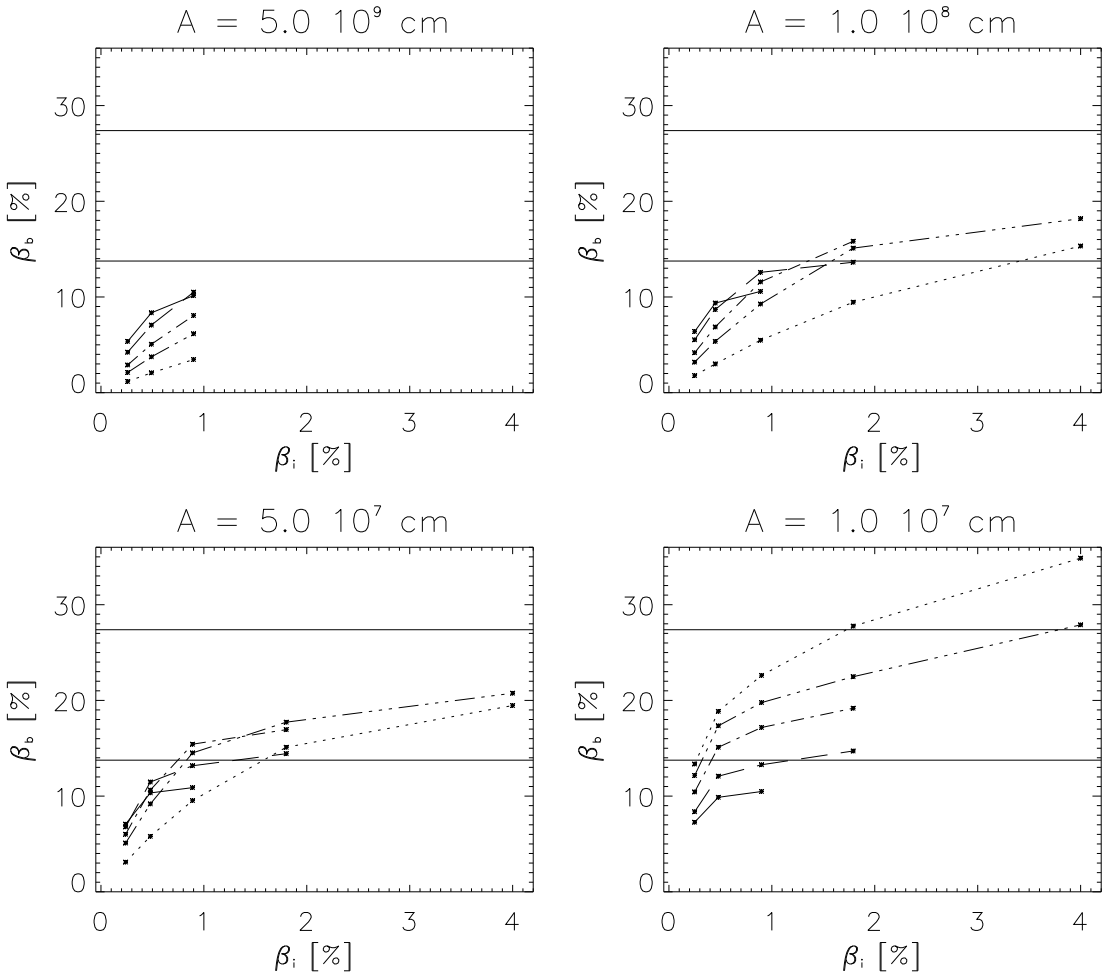

Fig. 3. Rotation rate parameter β_b at bounce as a function of the initial rotation rate β_i for different initial angular momentum distributions (separate panels) and different reduced adiabatic indices Γ_r: 1.325 (solid), 1.32 (dashed), 1.31 (dash dot), 1.30 (dash dot dot dot), 1.28 (dotted). The thin solid horizontal lines mark the critical values $\beta_{\rm sec}$ (lower line) and $\beta_{\rm dyn}$ (upper line), where MacLaurin spheroids become secularly and dynamically unstable against non-axisymmetric perturbations.

for about one millisecond. Moreover, all three models are quite extreme considering the region of the parameter space where likely initial models are supposed to be located. Realistic iron cores are probably rotating almost rigidly ($A \gtrsim 5\,10^7$ cm) and not very rapidly ($\beta_i \lesssim 1\,\%$). Hence, if the effective adiabatic index $\gtrsim$ 1.32, non-axisymmetric dynamical instabilities will not be encountered during core collapse.

4.7. Comparison with other investigations

Mönchmeyer et. al. (1991; see also Mönchmeyer 1993) investigated rotational core collapse using the iron core of an evolved 20 $M_\odot$star (Weaver et. al. 1985) as an initial model. Adding angular momentum to this spherical iron Mönchmeyer et. al. (1991) computed the core collapse of four models with different initial rotation rates and different initial angular momentum distributions. Their models A and B rotated according to a rotation law, which is identical to that of our models with A = A2. However, Mönchmeyer et. al. (1991) used $\Omega = \Omega(r)$, i.e., in their models (A and B) the angular velocity was constant on spheres (instead on cylinders). In their model D the rotation law was $\Omega = \Omega(\varpi)\, f(z)$, where $f(z)$ is a function depending weakly on the distance from the equatorial plane z. Finally, model C of Mönchmeyer et. al. (1991) initially rotated with $\Omega \propto [1 + \widetilde{\omega}/A]^{-1}$ with $A = 10^7$ cm. Although this rotation law has a different dependence on $\widetilde{\omega}$ than ours, the specific angular momentum distribution of model C is quite similar to that of our models with A =A3. Furthermore, there is no significant difference between models with A =A2 and A =A3 for the initial rotation rate of model C, which is β_i = 0.7 %.

The model sequence A, C, D, B (ordered by increasing β_i: 0.4%, 0.7%, 1.0%, 1.8%) has values of $\varrho_b, \beta_b, M_{ic}, \beta_{ic}, J_{ic}$ and E_{GW}, which are in between those of our sequences A1B(1 – 4)G1 and A1B(1 – 4)G2, respectively. Model C has been included, because there is no significant difference between models with A =A2 and A =A3 for an initial rotation rate β_i = 0.7 %. From the comparison one can conclude that the "exact" rotation law of the iron core is of less importance than the distribution

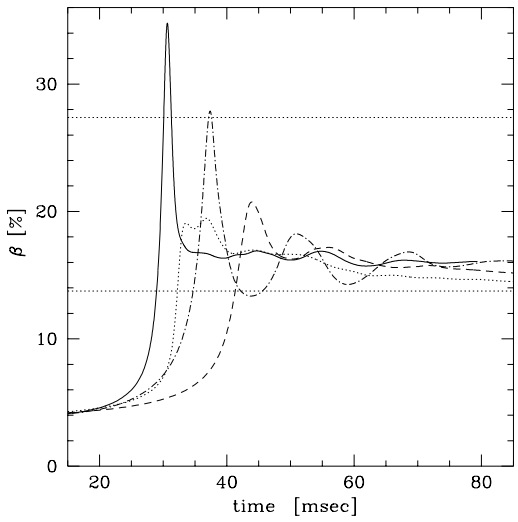

Fig. 4. Time evolution of the rotation parameter β for models A4B5G5 (solid), A4B5G4 (dash dot), A3B5G5 (dotted) and A3B5G4 (dashed). The dotted horizontal lines mark the critical values $\beta_{\rm sec}$ (lower line) and $\beta_{\rm dyn}$ (upper line), where MacLaurin spheroids become secularly and dynamically unstable against non-axisymmetric perturbations.

of angular momentum inside the core. Rigidly or almost rigidly rotating initial models where a large fraction of the total angular momentum is concentrated in the outer layers, and differentially rotating models where the angular momentum is concentrated in the center show similar dynamics when both have the same .

After bounce the four models of Mönchmeyer et. al. (1991) develop in a qualitatively different way than our models with the simplified equation of state. Hence, the parameters of the final equilibrium configurations do no longer fit in the range of polytropic models with $1.32 \lesssim \Gamma_r \lesssim 1.325$.

5. Results: the gravitational wave signal

The gravitational wave signature of axisymmetric rotational core collapse has been computed by various authors (Saenz & Shapiro 1978, 1981; Müller 1982; Finn & Evans 1990; Mönchmeyer et. al. 1991; Bonazzola & Marck 1993; Yamada & Sato 1995; Zwerger 1995; for a review see Bonazzola & Marck 1994 and Müller 1996).

The simulations of Mönchmeyer et. al. (1991) are the most realistic ones up to now. They used (i) an evolved iron core of a massive star (to which different amounts of rotation were added) as an initial model, (ii) employed a detailed equation of state, (iii) took electron captures into account and (iv) used a leakage scheme to describe the transport of neutrinos. Mönchmeyer et. al. (1991) simulated the evolution of four initial models and calculated their gravitational wave signature. An important result obtained by them was the discovery of the existence of two qualitatively different types of gravitational wave signals emitted during rotational core collapse.

So-called "standard" signals, or according to Mönchmeyer et. al. (1991) signals of type I, have been found by various authors (Müller 1982; Finn 1989; Finn & Evans 1990; Yamada & Sato 1995). They exhibit a large wave amplitude at bounce, which is followed by a ring-down of the signal, i.e., by post-bounce oscillations with decreasing amplitude. This ring-down is due to damped volume and surface oscillations of the inner core after bounce. Signals of type I are produced by cores bouncing at nuclear density or at low central densities when the ratio of (radial) kinetic energy to rotational energy is small. Signals of type II, which were first described by Mönchmeyer et. al. (1991), are characterized by several pronounced spikes, which arise if the core bounces more than once. Between the spikes the signal varies smoothly. Mönchmeyer et. al. (1991) could not clarify which conditions are sufficient for the appearance of a single dominant coherent volume mode causing the type II signal. Hence, they wondered whether such signals are only produced by models in a very narrow parameter range.

Of all the other investigations dealing with gravitational waves from rotational core collapse we only want to mention the results of Yamada & Sato (1995) here, because their approach has many similarities with ours. They also used polytropic models, a simplified equation of state whose stiffness was varied above nuclear matter density, Newtonian hydrodynamics and the quadrupole formula. Performing a set of nine collapse calculations of rotating polytropes, Yamada & Sato (1995) found that the peak amplitude of burst-like type I gravitational wave signals saturates for $q \gtrsim 0.5$, where $q = J/\frac{2GM}{c}$ is the dimensionless angular momentum of the core. They further noticed that the peak amplitude is sensitive to the stiffness of the equation of state just below nuclear matter density. They obtained maximum (dimensionless) wave amplitudes of $2\,10^{-24}$ for a source located at a distance of 10 Mpc. The maximum radiated energy was $10^{-10}\ M_\odot\, c^2$ and the typical frequency was several 100 Hz.

In the following two subsections we discuss the quadrupole waveforms and energy spectra of our models. The waveforms and energy spectra (as well as the evolution of the rotation rate parameter) of all models are available in digital and graphic form via the world wide web (**http://mpa-garching.mpg.de/~ewald/GRAV/grav.html**). Note in this respect that, due to an error in the data analysis program, the gravitational wave amplitudes and energies (total and spectral) given in Zwerger (1995) and in Müller & Zwerger (1995) are too large by a factor of two and four, respectively.

5.1. Quadrupole wave amplitudes

The evolution of the gravitational quadrupole wave amplitude $A_{20}^{\rm E2}$ (see Eq. 20; which is linked to h_+ via Eq. 21) can be divided into three distinct epochs corresponding to infall, bounce and post-bounce evolution, respectively (Finn 1989). Before bounce the collapse and the flattening of the rotating core leads to a monotonically increasing featureless positive wave amplitude in all of our models. The abrupt end of the collapse and the subsequent expansion of the core during core bounce gives rise to a rapidly changing quadrupole moment. Hence, the quadrupole wave amplitude rapidly rises shortly before bounce reaching a

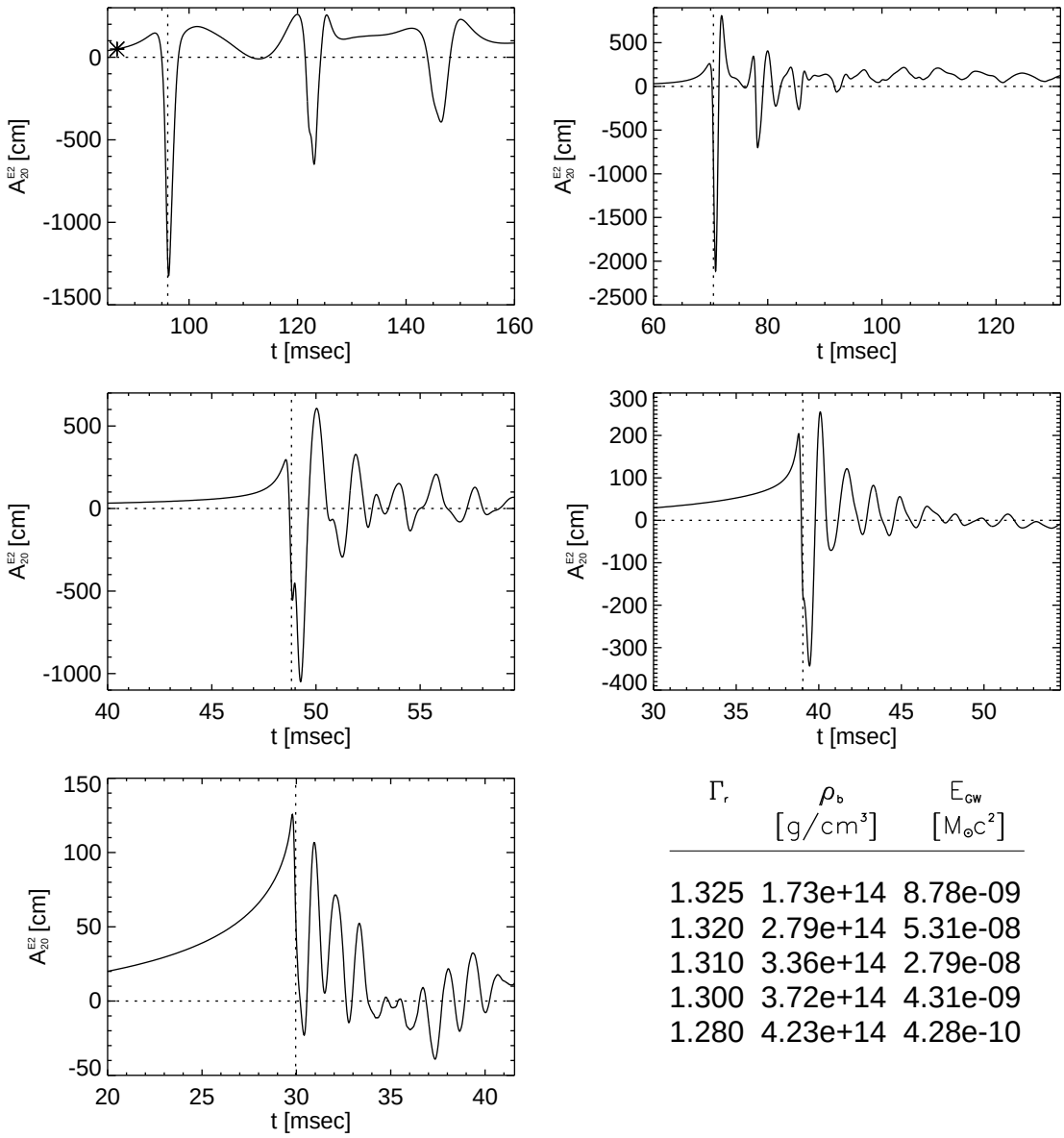

Fig. 5. Quadrupole amplitudes A_{20}^{E2} produced by the collapse of rotating polytropes with A = A1 = 5 10^9 cm and β_i = B3 = 0.009. In each panel the vertical dotted line marks the time of bounce. The adiabatic index Γ_1, the central density at bounce and the total amount of energy radiated in form of gravitational waves are given for each model (by the line from top to bottom) in the table in the lower right part of the figure.

local maximum with $A_{20}^{E2} > 0$ at $t_{max}^A < t^b$. Subsequently, the wave amplitude drops rapidly, becomes negative and exhibits a pronounced minimum at t_{min}^A (Figs. 5 and 6).

For most models, except those which initially rotate very differentially (A = 10^7 cm), we find $|A_{20}^{E2}(t = t_{min}^A)| > |A_{20}^{E2}(t = t_{max}^A)|$. The time interval $\Delta\tau_b \equiv t_{min}^A - t_{max}^A$ varies from 0.5 msec to 11 msec, but only in seven models $\Delta\tau_b > 5$ msec and just in two models $\Delta\tau_b > 7$ msec. Core bounce occurs during the rapid drop of the wave amplitude, i.e., $t_{max}^A < t_b < t_{min}^A$. A subset of models show an additional feature (a small peak) in their waveforms between $t_{\rm max}^A$ and $t_{\rm min}^A$ (see e.g., the middle two panels in Fig. 5). In these models the bounce occurs at the time of the local minimum before the small peak, which can be found in the parameter range A(1 – 3) B(1 – 3) G(1 – 4). Decreasing Γ_r the peak becomes smaller and eventually turns into a narrow shoulder in the waveform (see e.g., model A1B3G4; right middle panel in Fig. 5). The small peak or shoulder is not present in the waveforms of the models analyzed by Finn & Evans (1990), Mönchmeyer et. al. (1991) and Yamada & Sato (1995), but in those of Müller (1982).

During post-bounce evolution many of our models show the "standard" ring-down or type I waveform (Mönchmeyer et. al. 1991). According to our analysis there exists no one-to-one correspondence between extrema of the post-bounce gravita-

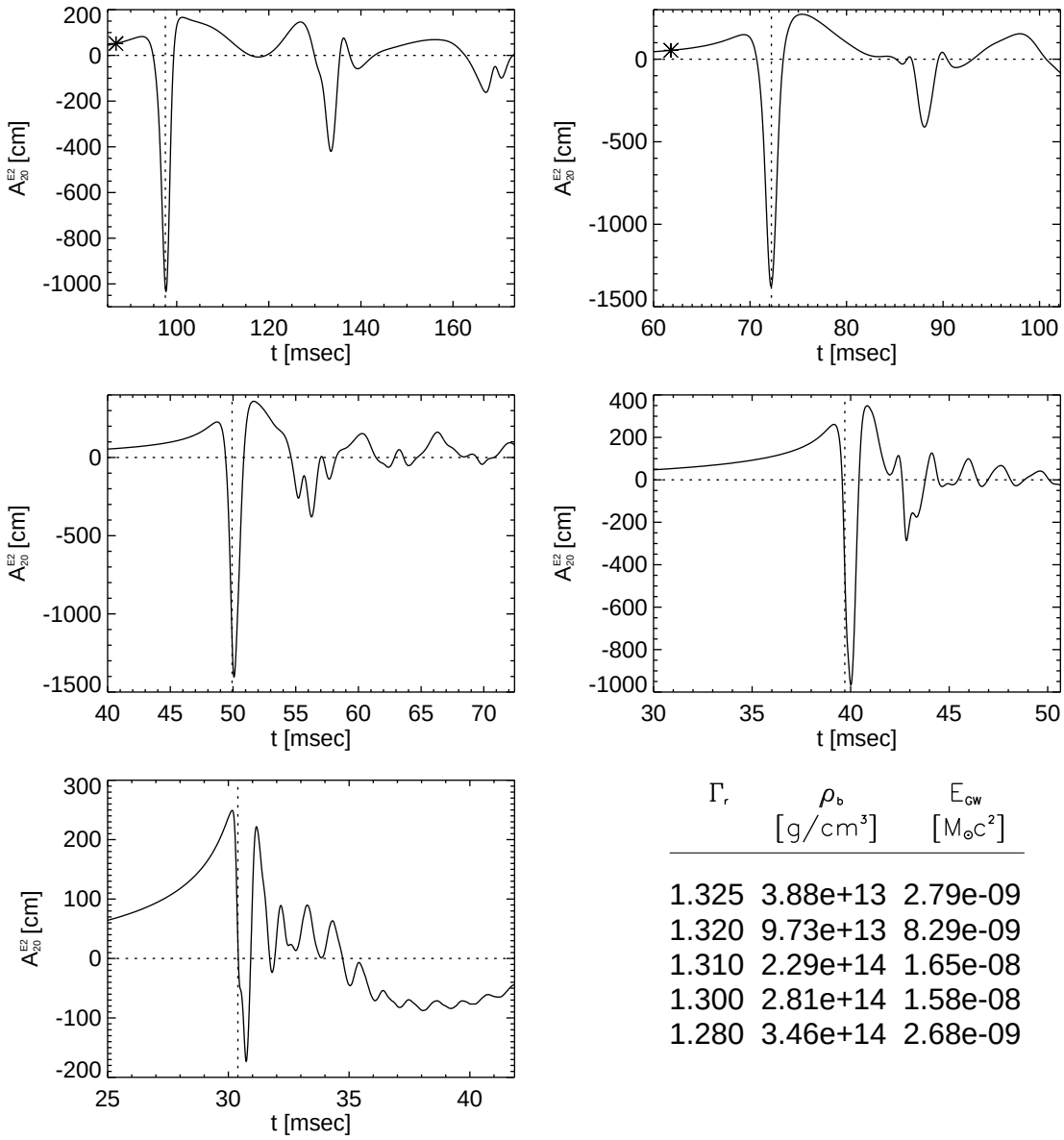

Γ_r	ρ_b [g/cm^3]	E_{GW} [$M_\odot c^2$]
1.325	3.88e+13	2.79e-09
1.320	9.73e+13	8.29e-09
1.310	2.29e+14	1.65e-08
1.300	2.81e+14	1.58e-08
1.280	3.46e+14	2.68e-09

Fig. 6. Same as Fig. 5 but for rotating polytropes with A = A3 = 5 10^7 cm and β_i = B3 = 0.009.

tional wave signal and extrema of the central density. Hence, the post-bounce variation of the quadrupole waveform does not result from a single dominant volume oscillation mode of the inner core, but is caused by a superposition of different volume and surface modes. We also find that the waveform maxima are usually more damped than the waveform minima during ring-down, because the temporal variation of the inner core's quadrupole moment is qualitatively different during phases of maximum compression and maximum expansion. During the latter phases the forces accelerating core matter are larger than during expansion phases, because they depend both on density and radius in a nonlinear way (Mönchmeyer 1993).

Among the models which have a value of the adiabatic index close to 4/3 ($\Gamma_r \geq 1.32$) we find type II gravitational wave signals (Mönchmeyer et. al. 1991). The waveform is characterized by several distinct waveform minima or spikes (top left panels in Figs. 5 and 6). Between the spikes the amplitude changes slowly on time scales that are significantly longer than the time interval given by the width of the spikes. The spikes are well correlated with the states of maximum compression of the inner core and hence are caused by repeated bounces of the inner core. The time interval between two spikes (or bounces) is typically longer than 10 msec, while it is less than 5 msec between post-bounce minima of type I signals.

Like Mönchmeyer et. al. (1991; see their model C) we also find models with gravitational wave signals intermediate between type I and type II (top right panel in Fig. 5). These intermediate waveforms are quite similar to type II signals, but the time interval between the spikes is reduced to 5–10 msec, and the waveform shows some structure between the spikes. De-

creasing the adiabatic index but keeping the initial rotation rate and rotation law fixed, we actually observe a gradual transition of the gravitational wave signal from type II to type I. This is illustrated in Figs. 5 and 6 for the model sequences A1B3G(1 – 5) and A3B3G(1 – 5), respectively.

Models with $\Gamma_r = 1.28$ and $A \geq 5\,10^7$ cm exhibit another yet unknown type of signal, which we will call a type III signal (left lower panels in Figs. 5 and 6). This signal type, which is not found in initially very differentially rotating models ($A = 107$ cm), shows no distinct spike, but is characterized by rapid (≈ 1 msec) post-bounce amplitude oscillations. Initially the time-averaged amplitudes are positive, but become negative during ring-down. The oscillations can not be assigned to oscillations of the central density, because the core soon reaches its post-bounce equilibrium in these models and the central density varies only slightly after bounce.

The gravitational wave signals of the four models (A-D) analyzed by Mönchmeyer et. al. (1991) fit in well to our set of models. Model A lies between our models A2B1G(1-2), which both emit a type I signal, and our models A2B2G(1-2), which produce a type II and and intermediate type signal, respectively. Model C is intermediate to our models A2B2G(1-2) and A2B3G(1-2), which all have type II signals, and model D falls between our latter two models. Finally, model B is bracketed by our models A2B4G(1-2), which both exhibit type I signals.

The signal forms, we have found, appear to be independent of the central density at bounce, except that the amplitudes become smaller for models that bounce at sub-nuclear densities. Definitely, the (mean) value of the effective adiabatic index is the crucial parameter determining the signal form. We further find that the wave amplitudes increase (decrease) with β_i for small (large) initial rotation rates $\beta_i \lesssim\%$. First the amplitudes become larger, because the deformation of the core and hence its quadrupole moment increases with the amount of rotation. But for sufficiently large rotation rates centrifugal forces become large enough to cause a bounce at sub-nuclear densities. Such a bounce occurs less abruptly than a bounce being caused by the stiffness of the nuclear equation of state, i.e., the acceleration forces are smaller in this case and consequently the wave amplitudes ($\propto$ second time derivative of quadrupole moment) are smaller, too. Along a model sequence of increasing β_i the maximum wave amplitude is obtained, when the density at bounce drops below nuclear matter density.

For models with $\Gamma_r \leq 1.31$ the signal strength becomes larger when one increases the initial degree of differential rotation (i.e., when one decreases A). In differentially rotating models more angular momentum is concentrated in the core's center than in rigidly rotating models with the same β_i. This gives rise to larger deformations and hence stronger signals (compare the signals of models A1B3G(3-5) and A3B3G(3-5) in Figs. 5 and 6). For $A \geq$ A2 the peak amplitudes vary only slightly with A. In models with $A =$ A4 the spike at bounce is very prominent. These models have an off-center density maximum at bounce, where the density reaches or even slightly exceeds nuclear matter density, while the central density stays up to two orders of magnitude below that value (see Table 3 and Sect. 4.3). The two models exceeding the stability limit for the onset of dynamical tri-axial instabilities (models A4B5G4 and A4B4G5) produce the largest amplitudes of all models.

Finally, we point out that the waveforms of all models significantly deviate from those obtained by Saenz & Shapiro (1978, 1981) for the collapse of homogeneous, rigidly rotating ellipsoids.

5.2. Energy spectra

Starting from Eq. (22) one can easily show that the spectral energy density of the quadrupole signal is given by

$$\frac{dE(\nu)}{d\nu} = \frac{c^3}{G}\,\frac{1}{16\pi}\,\nu^2\,\left|\widetilde{\mathrm{A}}_{20}^{\mathrm{E2}}(\nu)\right|^2 \tag{26}$$

where

$$\widetilde{\mathrm{A}}_{20}^{\mathrm{E2}}(\nu) = \frac{1}{\sqrt{2\pi}}\,\int_{-\infty}^{+\infty} \mathrm{A}_{20}^{\mathrm{E2}}(\mathrm{t})\,\mathrm{e}^{\mathrm{i}\nu\mathrm{t}}\mathrm{dt} \tag{27}$$

is the FOURIER transform of the quadrupole wave amplitude. As the wave amplitude is given at non-equidistant times due to the varying size of the hydrodynamic time step, we first had to interpolate the data onto an equidistant temporal grid, before we could perform the FOURIER transformation. A WELCH-window was applied in the FOURIER transformation to reduce the noise caused by the finite length of the wave signal (see Press et. al. 1990).

The total amount of energy radiated in form of (quadrupole) gravitational waves is given by

$$\mathrm{E_{GW}} = \int_0^{+\infty} \frac{\mathrm{dE}}{\mathrm{d}\nu}\,\mathrm{d}\nu. \tag{28}$$

This value should be identical to the value obtained from Eq. (22), where the integration is performed over time instead of frequency. Actually, we have used this equality to appropriately rescale the spectral energy density, which suffers from power losses due to the usage of the WELCH-window.

The energy spectra cover a frequency range of 50 Hz $\lesssim \nu \lesssim$ 3 kHz, but most of the power is emitted between 500 Hz and 1 kHz. Models bouncing at subnuclear densities have spectra, which drop extremely rapidly above 1 kHz, and models with a type II wave signal have spectra, which show characteristic oscillations (Fig. 7). These oscillations vanish when the signal type changes to type I. Moreover, a detailed analysis reveals that the oscillatory spectral component appears immediately after the second bounce. Additional bounces produce no new spectral features. They only increase the overall spectral power. The results further show that the spectra are neither very sensitive to β_i nor to the degree of differential rotation.

The total amount of energy radiated in form of gravitational waves lies in the range $6\ 10^{-11} M_\odot c^2 \lesssim E_{GW} \lesssim 8\ 10^{-8} M_\odot c^2$ (Tables 2 and 3). Most of this energy is emitted during the first oscillation of the inner core. Many models emit about 90 % and all models more than 2/3 of the total radiated energy before the central density reaches its second maximum. The radiated

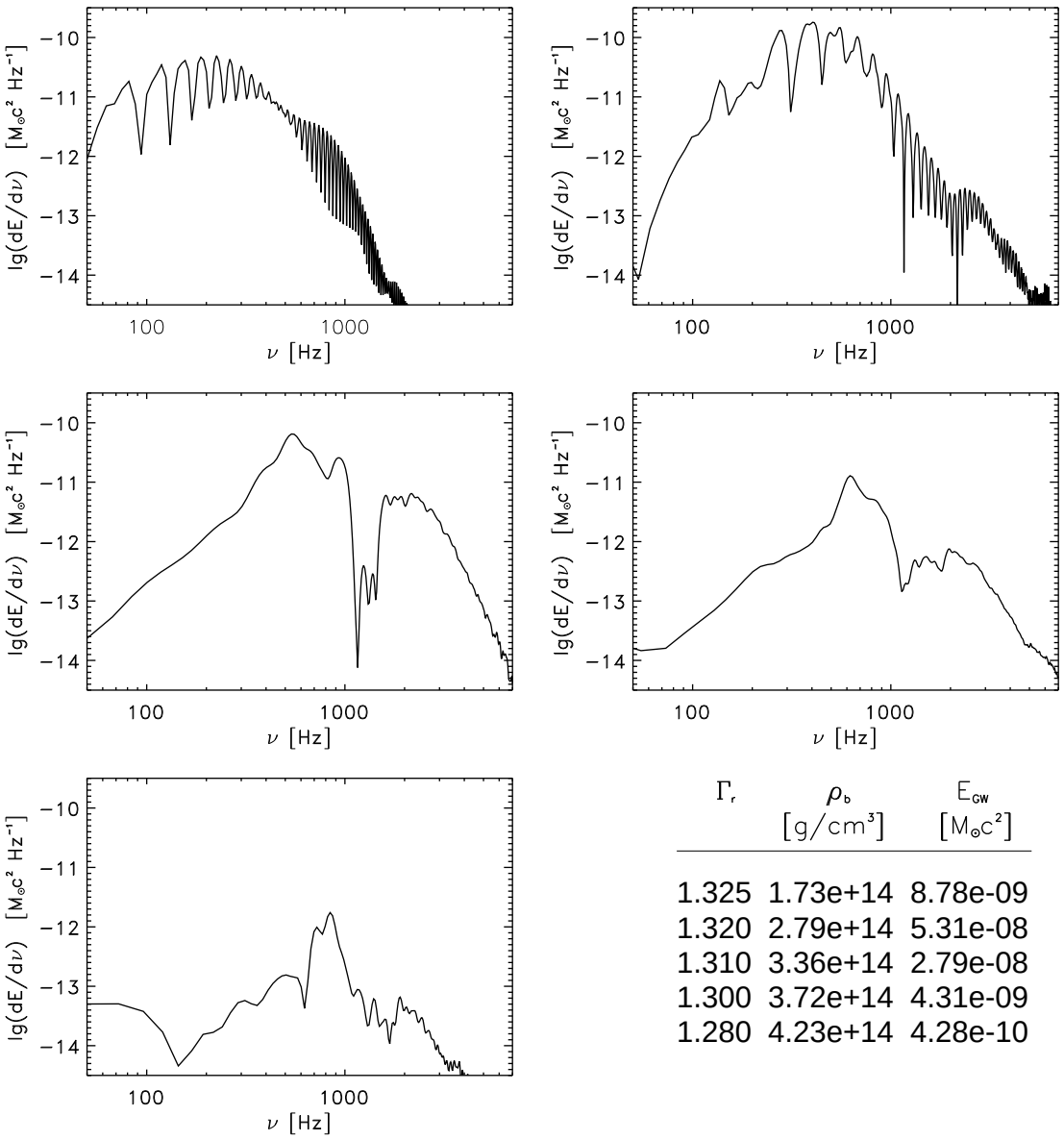

Γ_r	ρ_b [g/cm³]	E_{GW} [$M_\odot c^2$]
1.325	1.73e+14	8.78e-09
1.320	2.79e+14	5.31e-08
1.310	3.36e+14	2.79e-08
1.300	3.72e+14	4.31e-09
1.280	4.23e+14	4.28e-10

Fig. 7. Same as Fig. 5, but showing the spectral energy density $\mathrm{d}E/\mathrm{d}\nu$.

energy increases with increasing amplitude, and has a maximum for the same value of Γ_r as does the quadrupole wave amplitude. This maximum shifts to lower values of Γ_r with increasing initial rotation rate.

In Fig. 8 the (absolute values of the) maximum dimensionless gravitational quadrupole wave amplitude h^{TT} (see Eq. 21) of all models is plotted against frequency assuming a source located at a distance of 10 Mpc. The error bars mark the frequency range, which contains most of the spectral power (spectral energy density larger than 50% of maximum spectral power). There is a weak tendency that this dominant frequency range shifts to higher frequencies with decreasing Γ_r. The amplitudes of the four models calculated by Mönchmeyer et. al. (1991) are also shown in Fig. 8 and are marked by crosses.

Fig. 8 shows that the maximum wave amplitudes are in the range $4\ 10^{-25} \lesssim |h^{\mathrm{TT}}| \lesssim 4\ 10^{-23}$ (see also Tables 2 and 3). The largest signals are either produced by models which are initially slowly ($\beta_i \leq 0.9\,\%$) rotating and have an adiabatic index $\Gamma_r \geq 1.32$, or which are initially rapidly ($\beta_i \geq 1.8\,\%$) and strongly differentially ($A = 10^7$ cm) rotating and have a relatively small adiabatic index ($\Gamma_r \leq 1.30$). The first class of models experiences a bounce at densities above nuclear matter density with a fast deceleration of the collapsing core. This gives rise to a rapid change of the quadrupole moment of the core and consequently to a strong gravitational wave signal. In the other models the quadrupole moment is larger due to fast rotation, but changes less rapidly.

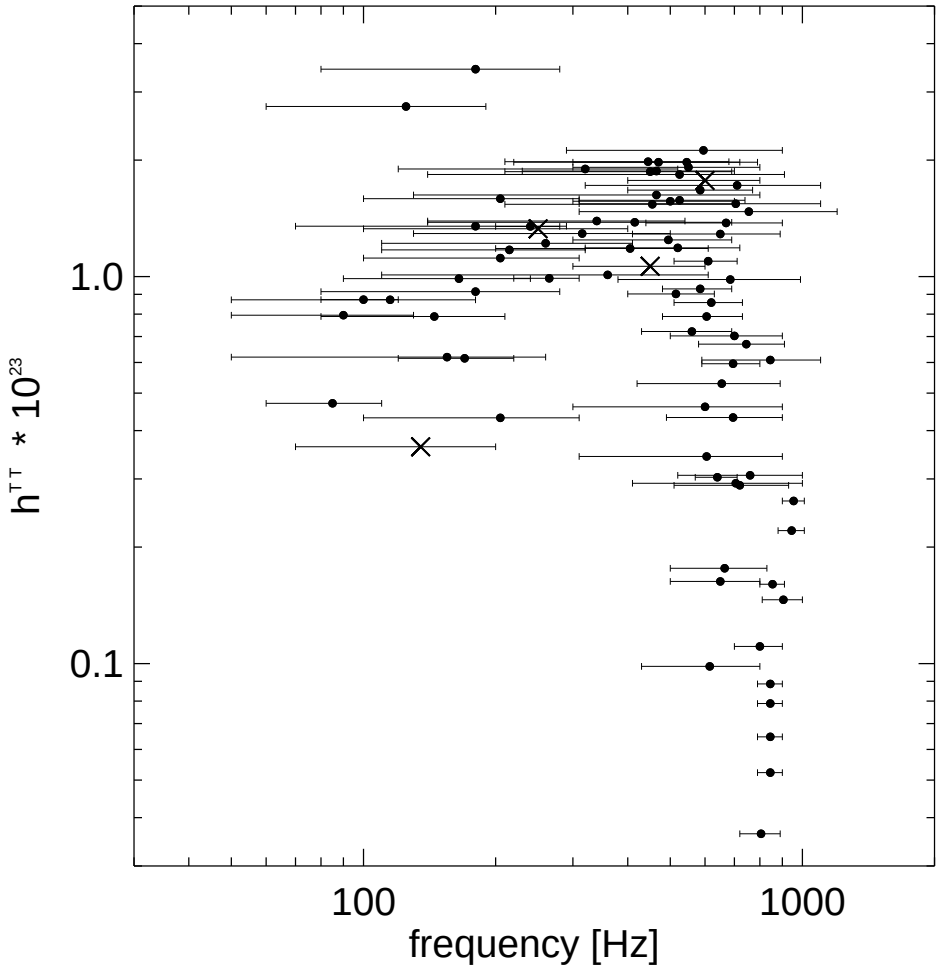

Fig. 8. The maximum dimensionless gravitational quadrupole wave amplitude $h^{\rm TT}$ of all models. The error bars give the frequency range, which contains most of the spectral power. It is assumed that the source is located at a distance of 10 Mpc. The amplitudes of the four models calculated by Mönchmeyer et. al. (1991) are also shown and are marked by crosses.

6. Summary and discussion

We have carried out a comprehensive parameter study of the dynamics of rotational core collapse in massive stars. The iron cores have been approximated by axisymmetric rotating $\Gamma = 4/3$ polytropes in rotational equilibrium. Any transport effects by neutrinos have been neglected. We have computed 18 initial models which differ by their amount of rotational energy and their distribution of angular momentum. The initial models range from slowly to rapidly rotating and from rigidly to extremely differentially rotating configurations. The collapse was induced by suddenly reducing the adiabatic index Γ to a value Γ_r with $1.28 \leq \Gamma_r \leq 1.325$. The stiffening of the equation of state at nuclear matter density and the thermal pressure in the matter heated by the prompt shock was simulated by means of a simplified analytic equation of state consisting of a polytropic and a thermal part. The evolution of a total of 78 models was followed well beyond core bounce using a two dimensional Newtonian hydrodynamic finite difference code.

A subset of models suffers a bounce caused by centrifugal forces at sub-nuclear densities. For a given rotation rate the bounce density decreases with increasing Γ_r and with increasing degree of differential rotation. Models suffering a bounce due to (or mainly due to) centrifugal forces show large amplitude oscillations of the inner core the central density varying by more than a factor of ten.

We have also calculated the gravitational (quadrupole) wave signal of the collapsing rotating cores. We find both type I (spike + ring-down) and type II (several distinct spikes) gravitational wave signals. Which type occurs is solely determined by the adiabatic index. Signals of type I are produced by models with a "soft" equation of state ($\Gamma_r \lesssim 1.31$), while signals of type II require a "stiff" equation of state ($\Gamma_r \gtrsim 1.32$). Decreasing the adiabatic index from 1.325 to 1.28 and keeping the other model parameters fixed, we observe a smooth transformation of the signal type. For Γ_r = 1.28 a third signal type is observed, which shows a large positive and a smaller negative wave amplitude just before and after bounce. Signals of type III are not found for extremely differentially rotating initial models.

The energy spectra cover a frequency range of 50 Hz $\lesssim \nu \lesssim$ 3 kHz most of the power being emitted between 500 Hz and 1 kHz. The spectra are neither very sensitive to the rotation rate nor to the degree of differential rotation. The total amount of energy radiated in form of gravitational waves lies in the range $6\ 10^{-11} M_\odot c^2 \lesssim E_{GW} \lesssim 8\ 10^{-8} M_\odot c^2$. The corresponding dimensionless wave amplitudes are in the range $4\ 10^{-25} \lesssim h \lesssim$

$4\ 10^{-23}$ for a source at a distance of 10 Mpc. The largest signals are either produced by models which are initially slowly rotating and have an adiabatic index $\Gamma_r \geq 1.32$, or which are initially rapidly and strongly differentially rotating and have a relatively small adiabatic index ($\Gamma_r \leq 1.30$).

Our comprehensive survey of rotational core collapse was only made possible, because we have restricted ourselves to simplified core models. The complicated micro-physics (electron captures and other weak interactions, equation of state) and neutrino transport processes have all been absorbed in one model parameter (Γ_r). Although this is an extreme simplification, we nevertheless think that it does not change the qualitative nature of our results. In particular, we do not expect that more realistic (axisymmetric) core collapse models will produce a significantly stronger gravitational wave signal than the "optimum" polytropic models in our survey. The investigated parameter space is so large that we most probably have covered all possible realistic collapse conditions. Larger initial rotation rates and lower values of the (effective) adiabatic index, which could lead to stronger gravitational wave signals, are most likely excluded. This is also supported by the fact that the signal strengths of the "realistic" models of Mönchmeyer et. al. (1991) agree well with those of our polytropic models.

A much more questionable simplification, however, is the use of Newtonian hydrodynamics, which should definitely be improved in future investigations. As is well known, general relativity has the tendency to destabilize stars and, in particular, compact objects (where GM/Rc^2 becomes comparable to unity). Because of general relativistic effects, the critical value of the adiabatic index, where a self-gravitating object becomes unstable against collapse, is increased relative to the Newtonian value of 4/3 (for non-rotating objects) to $\Gamma_{crit} = 4/3 + k\,(2GM/Rc^2)$ (see e.g., Tassoul 1978; Chap. 14.2). The (positive) constant k is of order unity and depends on the stratification of the object. Thus, general relativity counteracts the stabilizing influence of rotation. This implies that for the same initial conditions but taking relativistic effects into account, a bounce caused by rotation will occur at larger densities than in the Newtonian case. A centrifugally caused bounce might even change into a bounce caused by the stiffness of nuclear matter. Vice versa, relativistic models bouncing (due to rotation) at the same density than their Newtonian counterparts will posses a larger amount of rotational energy and will be more deformed.

The "softening" of the equation of state by relativistic effects can not be correctly modeled by reducing the value of Γ_r, because the strength of the relativistic effect depends on the time-dependent radial position in the core (while Γ_r is constant in time and throughout the core). For our models we find that $2GM/Rc^2 \lesssim 0.20$ at bounce, which shows that relativistic corrections to the critical adiabatic index can be quite large. Hence, in the future simulations of rotational core collapse, which we are planning to perform, we will take the relativistic effects into account.

In several models the rotation rate exceeds the critical value, where MacLaurin spheroids become secularly unstable against tri-axial perturbations ($\beta > \beta_{sec} \approx 0.14$). Two of the most differentially ($A = 10^7$ cm) and rapidly rotating ($\beta_i = 4\,\%$) models reach ($\Gamma_r = 1.30$) and even exceed ($\Gamma_r = 1.28$) the critical value for axisymmetric dynamical stability ($\beta > \beta_{dyn} \approx 0.27$). It has been have pointed out that if such instabilities indeed occur, a much stronger gravitational wave signal might be produced than by cores which remain axisymmetric during collapse (for a review, see e.g., Piran 1990; Thorne 1995).

According to this idea, the core will be transformed into a bar-like configuration that spins end-over-end like an American football. One has further speculated, whether the core might even break up into two or more massive pieces, if $\beta > \beta_{dyn}$. In that case the resulting gravitational radiation *could* be almost as strong as that from coalescing neutron star binaries (Thorne 1995). The strength of the gravitational signal sensitively depends on (i) the radius at which the centrifugal hang-up occurs and (ii) what fraction of the angular momentum of the non-axisymmetric core goes into gravitational waves, and what fraction into hydrodynamic waves. These sound and shock waves are produced as the bar or lumps, acting like a twirling-stick, plow through the surrounding matter.

Three-dimensional simulations of rotational core collapse, which can follow the growth of non-axisymmetric instabilities, have been performed by Bonazzola & Marck (1993, 1994) and Marck & Bonazzola (1993). They used a simplified two-index polytropic equation of state, which mimics the realistic equation of state, and computed the evolution of several initial models. They found that the wave amplitude is within a factor of two of that of 2D simulations for the same initial deformation of the core (Bonazzola & Marck 1994). As the, up to now unique, 3D calculations of Bonazzola & Marck have been restricted to a small fraction of the parameter space, we (Rampp, Ruffert & Müller in preparation) have begun an investigation to explore non-axisymmetric instabilities of collapsing, rapidly rotating cores and to compute the resulting gravitational wave signal. The results from this project will be presented elsewhere.

Acknowledgements. We would like to thank Thomas Janka, Markus Rampp, Maximilian Ruffert, Gerhard Schäfer and Bernard Schutz for many enlightening discussions and valuable comments. All hydrodynamic simulations were performed on the CRAY-YMP and the CRAY-JEDI of the Rechenzentrum Garching.

References

Bethe, H. A. *Rev. Mod. Phys.* **62** (1990) 801.
Blanchet, L., Damour, T., Schäfer, G., *MNRAS* **242** (1990) 289.
Bonazzola, S., Marck, J.-A., *A&A* **267** (1993) 623.
Bonazzola, S., Marck, J.-A., *Ann. Rev. Nucl. Part. Sci.* **45** (1994) 655.
Bruenn, S.W., Nuclear Physics in the Universe (eds. M. W. Guidry and M. R. Strayer, Inst. of Physics, Bristol, 1993) p. 31.
Colella, P., Woodward, P.R., *J. Comput. Phys.* **54** (1984) 174.
Endal, A.S., Sofia, S., *Phys. Rev. Lett.* **39** (1977) 1429.
Eriguchi, Y., Müller, E., *A&A* **147** (1984) 161.
Finn, L.S., Frontiers in Numerical Relativity (eds. C.R. Evans, L.S. Finn, and D.W. Hobill, Cambridge Univ. Press, 1989) p. 126.
Finn, L.S., Evans, C.R., *ApJ* **351** (1990) 588.

Fryxell, B.A., Müller, E., Arnett, W. D., Report MPA449, Max-Planck-Institut für Astrophysik, Garching, 1989.
Goldreich, P., Weber, S.V., *ApJ* **238** (1980) 991.
Hillebrandt, W., Wolff, R. G., Nucleosynthesis (eds. W.D. Arnett and J.W. Truran, Univ. Chicago Press, Chicago, 1995) p. 131.
Janka, H.-Th., Zwerger, T., Mönchmeyer, R., *A&A* **268** (1993) 360.
Lattimer, J.M., Swesty, F.D., *Nucl. Phys.* **A535** (1991) 331.
LeBlanc, J.M., Wilson, J.R., *ApJ* **161** (1970) 541.
Ledoux, P., *ApJ* **102** (1945) 143.
Marck, J.-A., Bonazzola, S., Approaches to Numerical relativity (ed. R. D'Inverno, Cambridge Univ. Press, Cambridge, 1992) p. 247.
Mönchmeyer, R., *Ph.D. thesis*, Technical University München, 1993, unpublished.
Mönchmeyer, R., Schäfer, G., Müller, E., Kates, R., *A&A* **246** (1991) 417.
Müller, E., *A&A* **114** (1982) 53.
Müller, E., *J. Phys. G* **16** (1990) 1571.
Müller, E., Proc of the 1995 Les Houches Summer School on *Astrophysical Sources of Gravitational Radiation*, eds. J.-A. Marck and J.-P. Lasota, Cambridge Univ. Press, 1996, in press
Müller, E., Hillebrandt, W., *A&A* **103** (1981) 358.
Müller, E., Janka, H.-Th., *Astron. Astrophys.*, in press; and Report MPA927, Max-Planck-Institut für Astrophysik, Garching, 1996.
Müller, E., Steinmetz, M., *Comp. Phys. Comm.* **89** (1995) 45.
Müller, E., Zwerger, T., *Ann. N.Y. Acad. Sci.* **759** (1995) 498.
Müller, E., Różyczka, M., Hillebrandt, M., *A&A* **81** (1980) 288.
Nakamura, T., Oohara, K., Frontiers in Numerical Relativity (eds. C.R. Evans, L.S. Finn, and D.W. Hobill, Cambridge Univ. Press, 1989) p. 254.
Piran, T., Supernovae (eds. J.C. Wheeler, T. Piran and S. Weinberg, World Scientific, Singapore, 1990) p. 303.
Press, W.H., Flannery, B.P., Teukolsky, S.A., Vetterling, W.T., Numerical Recipes. The Art of Scientific Computing (Cambridge University Press, Cambridge, 1990) p. .
Saenz, R.A., Shapiro, S.L., *ApJ* **221** (1978) 286.
Saenz, R.A., Shapiro, S.L., *ApJ* **244** (1981) 1033.
Shapiro, L.S., Teukolsky, S.A., *ApJ* **207** (1976) 263.
Shapiro, L.S., Teukolsky, S.A., Black Holes White Dwarfs and Neutron Stars (John Wiley & Sons, New York, 1983) p. .
Symbalisty, E., *ApJ* **285** (1984) 729.
Tassoul, J.-L., Theory of Rotating Stars (Princeton Univ. Press, New Jersey, 1978).
Thorne, K.S., *Rev. Mod. Phys.* **52** (1980) 299.
Thorne, K.S., Proc. of the Snowmass 95 Summer Study on *Particle and Nuclear Astrophysics and Cosmology*, eds. E.W. Kolb and R. Peccei, World Scientific, Singapore, 1995, in press.
Tohline, J.E., *ApJ* **285** (1984) 721
Tohline, J.E., Schombert, J.M., Boss, A.P., *Space Sci. Rev.* **27** (1980) 555.
van Riper, K.A., Lattimer, J.M., *ApJ* **249** (1982) 270.
Weaver, T.A., Woosley, S.E., Fuller, G.M., Numerical Astrophysics (eds. J.M. Centrella, J.M. LeBlanc and R.L. Bowers, Jones and Bartlett, Boston, 1985) p. 374.
Wilson, J.R., Numerical Astrophysics (eds. J. M. Centrella, J. M. LeBlanc and R.L. Bowers, Bartlett, Boston, 1985) p. 422.
Yahil, A., *ApJ* **265** (1983) 1047.
Yamada, S., Sato, K., *Astrophys. J.* **434** (1994) 268.
Yamada, S., Sato, K., *Astrophys. J.* **450** (1995) 245.
Zwerger, T., *Ph.D. Thesis*, Technische Universität München, 1995, unpublished.

This article was processed by the author using Springer-Verlag LaTeX A&A style file *L-AA* version 3.